Global Biogeochemical Cycles

RESEARCH ARTICLE
10.1029/2020GB006758

Global Coordination in Plant Physiological and Rooting Strategies in Response to Water Stress

Yaling Liu[1], Alexandra G. Konings[2], Daniel Kennedy[3], and Pierre Gentine[1]

[1]Earth and Environmental Engineering Department, Columbia University, New York, NY, USA, [2]Department of Earth System Science, Stanford University, Stanford, CA, USA, [3]National Center for Atmospheric Research, Boulder, CO, USA

Key Points:

- Plants with deeper roots maintain relatively steady nighttime vegetation optical depth (VOD) and taller plants drop daytime VOD more
- Physiological regulation is the dominant strategy in Northern high latitudes, but it couples with deep rooting in the tropics, Eastern US
- Grassland areas in the Western US, Central Asia, Northeastern China, and Mongolia Plateau lack strategies for water stress

Supporting Information:

Supporting Information may be found in the online version of this article.

Correspondence to:

Y. Liu,
yl3937@columbia.edu

Citation:

Liu, Y., Konings, A. G., Kennedy, D., & Gentine, P. (2021). Global coordination in plant physiological and rooting strategies in response to water stress. *Global Biogeochemical Cycles*, *35*, e2020GB006758. https://doi.org/10.1029/2020GB006758

Received 30 JUL 2020
Accepted 28 MAY 2021

Abstract Plants employ a range of strategies to modulate the impact of water stress, including changes to rooting depth and hydraulic conductance (e.g., xylem conductance). However, it is still poorly understood how these strategies vary in relation to climate and land cover types and how they could coordinate globally. Based on daily microwave vegetation optical depth (VOD) from AMSR-E and AMSR2 over 2002–2011, we estimate two proxies for stress regulation: (a) an effective plant rooting depth $\left(Z_r^*\right)$ and (b) the effective plant hydraulic conductance $\left(\mathrm{K}_{\mathrm{plant}}^*\right)$ to delineate two strategies: deep rooting and strong physiological regulation. We find that plants with deeper Z_r^* (e.g., evergreen/deciduous broadleaf forest) are mostly distributed in warm or wet regions, and maintain a relatively steady nighttime VOD because of access to deeper water. Taller plants exhibit greater drop in daytime VOD due to their greater physiological vulnerability. While physiological regulation appears to be the dominant water stress regulation strategy at Northern high latitudes where open shrubland and (woody) savannas are distributed, this physiological regulation is coupled with deep rooting in forest and (woody) savanna areas in the tropics, Eastern US, and Southeastern China. Meanwhile, grasslands in the Western US, Central Asia, Northeastern China, and Mongolia Plateau may be the regions most susceptible to water stress impact because neither water stress mitigation strategy is present. This new framework paves the road for a better understanding of plant water stress strategies at the global scale, and for enhancing large-scale drought prediction and drought impact assessment in Earth system models by improving plant water stress response.

1. Introduction

Drought is a widespread environmental stress occurring across the globe (Aroca, 2012). It is projected to intensify in frequency and severity and propagate via land-atmosphere feedbacks in a warming climate, posing serious threats to future ecosystem services and food security (Farooq et al., 2009; Lipiec et al., 2013; Miralles et al., 2018; Zhou et al., 2019). For instance, drought-induced forest decline could convert tropical forests from a net carbon sink into a carbon source during this century (Hubau et al., 2020; Lewis, 2006). Thus, a good understanding of plant response to water stress is crucial to understanding future ecosystem changes and continental carbon uptake.

Droughts can cause severe plant water stress, limiting plant growth through impaired enzyme activities, loss of turgor, and decreased energy supply (Taiz & Zeiger, 2010). Droughts also limit nutrient uptake (Matsui & Singh, 2003; Subramanian et al., 2006) and thus may cause pronounced reduction in productivity. Droughts can even trigger mortality at regional and continental scales (Allen et al., 2010; Aroca, 2012; Choat et al., 2018), resulting in changes in vegetation composition and structure. During periods of water stress, low soil water content and high evaporative demand induce a decrease in plant water potential and an increase in the hydraulic resistance along the soil-plant water continuum (Bartlett et al., 2016; Bréda et al., 2006). As a result (partial) stomatal closure may occur, and when water stress intensifies sufficiently, the water transport in the xylem tissues may be irreversibly disrupted due to water cohesion break-down and massive embolism, which injures plants and may ultimately cause mortality (Bartlett et al., 2016; Bréda et al., 2006; Choat et al., 2018).

Plants, however, employ not a single but a wide range of strategies, including physiological, morphological, anatomical, and biochemical changes, to escape, avoid, or tolerate water stress (Aroca, 2012; Choat et al., 2018; Salehi-Lisar & Bakhshayeshan-Agdam, 2016). For example, plants avoid water stress by either taking up more water through the roots or by minimizing water loss through transpiration (Blum, 2005).

This is accomplished through a range of morphological and physiological changes, such as developing deeper roots and stimulating root proliferation to access deeper soil water (Giardina et al., 2018; Gowda et al., 2011; Matsui & Singh, 2003; Nardini et al., 2016), increasing stomatal and cuticular resistance (Hochberg, Windt, et al., 2017; Martin-StPaul et al., 2017; Sinclair & Muchow, 2001), among others.

Despite the many efforts devoted to understanding plant strategies to water stress, few studies have scrutinized this topic at the ecosystem scale using an integrated perspective considering both physiological and rooting regulations. For instance, a key component of ecosystem water stress—the sensitivity of stomatal conductance (g_s) to water stress—is usually implemented in land-surface models (LSMs) and hydrological models empirically as a function of root zone soil moisture and vapor pressure deficit (Ball et al., 1987; Jarvis, 1976), typically ignoring the role of plant hydraulics (water movement through the plant) and associated changes in leaf and xylem water potential that have a more intrinsic connection with stomatal regulation (Bartlett et al., 2016; McDowell & Allen, 2015; Sperry & Love, 2015). The plant hydraulic system, however, maintains a balance between water supply and demand, which are determined by both hydraulic conductance (K) and g_s (Martínez-Vilalta et al., 2014; Sperry & Love, 2015). Despite the progress in process-level understanding of plant hydraulics in recent years, only very few land-surface models have incorporated a plant hydraulics scheme representing the response of plant water and CO_2 fluxes to both soil and atmospheric water deficits (Bonan et al., 2014; Christoffersen et al., 2016; Kennedy et al., 2019; Mackay et al., 2015; Xu et al., 2016). This lack of physically based water stress representation can result in substantial carbon cycle uncertainty (Green et al., 2019; Trugman et al., 2018). Furthermore, incorrect parameterization of plant water stress can lead to erroneous seasonal and interannual dryness and drought response in Earth system models (Green et al., 2017).

Additionally, most previous studies on plant strategies to water stress have been based on in-situ measurements or laboratory experiments for an individual or a few plants, often at the species level. However, where these strategies are deployed at a regional and global scale and how plants coordinate these strategies under different climate and ecosystem regimes are still unknown. Recent work has demonstrated the potential use of microwave vegetation optical depth (VOD) data to assess the variability of leaf water potential (Konings & Gentine, 2017; Konings, Williams, & Gentine, 2017; Momen et al., 2017). Thus, VOD holds great promise in unraveling plants' responses to water stress at large scales. The use of remote sensing data is additionally advantageous as these data naturally integrate variability across species in a multispecific landscape, providing estimates of effective ecosystem behavior at scales relevant to those at which land-surface models operate. In forests, hydraulic diversity has been shown to affect ecosystem drought response (Anderegg et al., 2018), thus, studying the distribution of the integrated ecosystem-average behavior (instead of say, just the most dominant trees in each location) is crucial for correctly capturing spatial variability in plant water response.

This work is motivated by filling this knowledge gap and evaluating where different plant water strategies take place and how they coordinate globally. We aim to analyze, for the first time, the global dominance and coordination of plant strategies for different ecosystems and climate conditions. Specifically, based on a water mass balance equation (Lyon et al., 2015; Teuling et al., 2006) and microwave VOD measurements (Du et al., 2017) that are related to leaf water potential, we estimate two water-stress proxies: (1) an effective plant rooting depth $\left(Z_r^*\right)$ and (2) a whole plant hydraulic conductance $\left(\mathrm{K}_{\mathrm{plant}}^*\right)$. These two proxies are used here to exemplify the morphological and physiological strategies that plants employ to withstand water stress. By combining the two proxies, we then examine where each of the two strategies, deep rooting or physiological regulation, dominate the response to water stress and how they coordinate globally.

We focus on these two strategies mainly because (1) they are commonly deployed by plants to cope with water stress, (2) current data availability allow us to scrutinize them at a global scale, and (3) they can be implemented in LSMs. We note that the physiological regulation we examine here is an integrated reflection of plant physiological responses to water stress, which may encompass a series of processes as mentioned before. Examination of molecular/cellular level strategies (e.g., aquaporins, stress proteins) at global scale is infeasible at this stage despite their importance. The same philosophy applies to the fact that we focus only on rooting depth here, rather than on other possible morphological or root-related strategies (e.g., hydraulic lift, root area). Furthermore, vegetation rooting depth is one of the main regulators of water and nutrient uptake by plants (Fan et al., 2017; Jackson et al., 1996; Schenk & Jackson, 2002). In other words, the two

proxies are used here to exemplify the morphological and physiological strategies that plants employ to withstand water stress.

2. Methods and Data

2.1. Methods

For both of the proxies derived below, a series of data processing procedures are used to filter data in order to identify a time window for each year when biomass variation is minimal and soil is drying. The readers are referred to Section S1.1 of the supporting information for detailed description of the data filtering (see also Figure S1).

2.1.1. Estimating the Proxy of Rooting Depth

To evaluate the role of rooting depth in the plants' response to water stress, a hydrologically effective Z_r is calculated per pixel. Current available global gridded rooting depth datasets are either simulated from models (Fan et al., 2017; Kleidon, 2004; Yang et al., 2016) or upscaled from in-situ observations (Schenk et al., 2009). These approaches have inherent sources of uncertainty: (a) model simulations may have large uncertainties due to the use of multiple assumptions about soil physics and lack of adequate parameterization, including poor or no representations of variations in other water stress response strategies (such as physiological regulation through plant hydraulics) that are likely coordinated with rooting strategies and (b) the limited Z_r observations used for upscaling are usually only representative of a few plants and local conditions which may differ greatly from the grid level effective Z_r (Yang et al., 2016).

To overcome these issues, we derive a proxy of Z_r (hereafter denoted as Z_r^*) that is connected with physiological regulations by using the day-to-day variations in nighttime VOD variations in combination with a water balance equation. Though our proxy also depends on simplified assumptions (see Equations 1–8 below) that may lead to uncertainties in the estimated Z_r^*, we believe it still represent an important first step toward a global assessment of water strategies. It is a useful proxy for global rooting depth assessment because (a) the VOD data are retrieved consistently from satellite observations, globally, and sensitive to plant water content and thus plant water strategies, (b) the proxy is derived from a simple water balance which provides a physical ground for the estimation, and (c) the proxy of rooting depth is derived from VOD, which is also used to derive another proxy for K_{plant} (using the within day variations as opposed to day-to-day nighttime variations), thus the two proxies are inherently linked through VOD.

Our strategy for the retrieval is as follows. During dry-downs, we assume that runoff is small within the studied period, so that variations in soil moisture can be represented with a simplified water balance (Teuling et al., 2006):

$$Z_r \cdot \frac{d\theta}{dt} = \mathrm{P} - \mathrm{ET} \tag{1}$$

where θ is volumetric soil moisture content across the root-zone ($m^3\ m^{-3}$), and t represents time, and P and ET are precipitation and evapotranspiration, respectively. Given daily P and ET (here based on reanalysis data), we only need the soil moisture change rate (i.e., $\frac{d\theta}{dt}$) to derive an estimate for Z_r. At predawn, as transpiration ceases and water storage flow is minimal, an equilibrium is typically observed in the soil-plant-atmosphere continuum (SPAC) of water potentials—leaf water potential (ψ_L) thus equals root zone soil water potential (ψ_s) minus gravity pull (neglected here) (Sellin, 1999). It is assumed that an equilibrium in the SPAC is already achieved by 1:30 a.m. (the time of satellite overpass). That is, we assume changes in predawn ψ_L (hereafter denoted as ψ_{L_pd}) are equal to and track those in root zone predawn ψ_s (ψ_{s_pd}):

$$\frac{d\psi_{L\_pd}}{dt} = \frac{d\psi_{s\_pd}}{dt} \tag{2}$$

We then simply assume a near-linear relationship between predawn $\psi_s$and root zone soil moisture θ to derive the changes in $\frac{d\theta}{dt}$:

$$\frac{d\theta_{pd}}{dt} \propto \frac{d\psi_{s\_pd}}{dt} \tag{3}$$

where θ_{pd} and ψ_{s_pd} denote predawn θ and ψ_s, respectively. Thus if we can derive $\frac{d\psi_{s\_pd}}{dt}$ from observational VOD data, it can be used as a proxy of $\frac{d\theta_{pd}}{dt}$. To do so we use the typical assumption of a linear relationship between leaf water potential (ψ_L) and VOD (Konings & Gentine, 2017), which is reasonably away from the turgor loss point (Lambers & Oliveira):

$$\mathrm{VOD} = \alpha \cdot \psi_L + \beta \tag{4}$$

where α and β are empirical coefficients. Thus, we have:

$$\frac{dVOD_{pd}}{dt} = \alpha \cdot \frac{d\psi_{L\_pd}}{dt} \tag{5}$$

Since α is constant, by combining Equations 2, 3 and 5 we then have:

$$\frac{dVOD_{pd}}{dt} \propto \frac{d\psi_{L\_pd}}{dt} \propto \frac{d\theta_{pd}}{dt} \tag{6}$$

Finally, the nighttime VOD can be used to indirectly infer variations in root zone soil moisture $\left(\frac{d\theta_{pd}}{dt}\right)$. The VOD_{pd} time series therefore allow us to calculate $\frac{dVOD_{pd}}{dt}$, which can be used as a surrogate of $\frac{d\theta_{pd}}{dt}$, and then by plugging it into Equation 1 we will have:

$$Z_r \propto \frac{P - ET}{\frac{dVOD_{pd}}{dt}} \tag{7}$$

Then, we can explicitly derive the Z_r proxy (denoted here as Z_r^*) as:

$$Z_r^* = \frac{P - ET}{\frac{dVOD_{pd}}{dt}} \tag{8}$$

We note that the assumption on a near linear relationship between water potential and root zone moisture (Equation 3) can be relaxed by using a non-linear pedotransfer function (Saxton et al., 1986) for Z_r^* estimation—it does not change the main conclusions reached here. Although potentially more precise mathematically, this method has the disadvantage of introducing uncertainties related to the specification of the retention curves. We therefore do not use the nonlinear retention curve-based proxy in our baseline results. Nevertheless, for completeness, a detailed description for the second approach is documented in Section S1.2 of the supporting information.

We note that the Z_r^* estimated herein provides a scale of the effective rooting depth at a 0.25° horizontal grid unit—it is proportional to the effective rooting depth. In fact, the effective rooting depth itself does not represent the actual rooting depth of any individual plants within the grid unit, but assumes that all individual plants within a grid cell behave collectively to withdraw soil water to meet the grid-level transpiration demand.

2.1.2. Estimates of Physiological Effects

There are a variety of plant physiological responses to water stress (Section 1), here we use a proxy—the difference between daily predawn VOD ($\mathrm{VOD_{pd}}$) and midday VOD ($\mathrm{VOD_{md}}$) (hereafter denoted as "$\mathrm{VOD_{diff}}$"), which reflects daily variations in leaf water content and potential—to exemplify their integrated physiological effects. When strong physiological regulation takes place during water stress, $\mathrm{VOD_{diff}}$ is generally

expected to be small, as the plant either continues to efficiently use water from the soil or from internal storage or because it limits water loss by reducing stomatal conductance to prevent the hydraulic dysfunction associated with substantial drops in xylem and leaf water potentials (Aroca, 2012; Choat et al., 2018; Taiz & Zeiger, 2010).

As discussed in Momen et al. (2017) and Zhang et al. (2019), VOD varies with both leaf water potential and biomass (including phenological changes). Furthermore, even at a given level of biomass, the linearized relationship between VOD and ψ_L varies in space depending on vegetation structure (Konings & Gentine, 2017). To minimize the effects of (dry) biomass on VOD, we normalize VOD_{diff} by VOD_{pd}, that is, we focus on the relative water content change rather than the absolute value which scales with total biomass. Furthermore, minimal drops in VOD_{diff}/VOD_{pd} in tropical rainforests (high evaporative demand) compared to similar drops in boreal forests at high latitudes (low evaporative demand) would have very different meanings on plant hydraulics given the large differences in atmospheric evaporative demand. Thus VOD_{diff}/VOD_{pd} needs to be further normalized by the (grid-level) plant water use, ET, to correctly understand the plant's resistance to leaf water potential drop. Thus, we consider the ratio $VOD_{diff}/VOD_{pd}/ET$, which is more directly linked to plant traits and less influenced by climate than isohydricity (Hochberg, Rockwell, et al., 2017). Importantly, this parameter is closely related to whole plant hydraulic resistance R_{plant} (reciprocal of the hydraulic conductance K_{plant}) (Sack & Holbrook, 2006) defined as:

$$R_{plant} = \frac{\psi_s - \psi_L}{Tr} \tag{9}$$

$$K_{plant} = \frac{1}{R_{plant}} \tag{10}$$

where Tr stands for transpiration.

Given VOD is both determined by (dry) aboveground biomass (AGB) and ψ_L, and the relationship between ψ_L and relative water content (RWC, mass of water per unit mass of dry AGB) could be linearized (Momen et al., 2017), then their relationship can be represented as:

$$VOD = b \cdot AGB \cdot RWC \tag{11}$$

$$dRWC \propto d\psi_L = \psi_{L\_pd} - \psi_{L\_md} \tag{12}$$

where b is a coefficient depending on canopy structure. Given Equation 11, we will have:

$$dRWC = \frac{VOD_{pd} - VOD_{md}}{b \cdot AGB} \tag{13}$$

As indicated by (Zhang et al., 2019), VOD is mostly determined by AGB rather than ψ_L, then:

$$\frac{VOD_{pd} - VOD_{md}}{b \cdot AGB} \propto \frac{VOD_{pd} - VOD_{md}}{VOD_{pd}} \tag{14}$$

In addition, Zhang et al. (2019) reveals that VOD_{md}/VOD_{pd} can be used to assess ψ_L variations to soil dry down (i.e., $\psi_{L\_pd} - \psi_{L\_md}$), and by combining Equations 12–14 then we could have:

$$\frac{VOD_{pd} - VOD_{md}}{VOD_{pd}} = \frac{VOD_{diff}}{VOD_{pd}} \propto \psi_{L\_pd} - \psi_{L\_md} \tag{15}$$

Thus, we use VOD_{diff}/VOD_{pd} as a surrogate for $\psi_s - \psi_L$ in Equation 9, and if we use ET instead of transpiration, then we will have:

$$R_{plant} \propto \frac{\frac{VOD_{diff}}{VOD_{pd}}}{ET} \tag{16}$$

Thus, the index $VOD_{diff}/VOD_{pd}/ET$ can be viewed as a proxy for R_{plant} (denoted here as R^*_{plant}), evaluated at ecosystem scale:

$$R^*_{plant} = \frac{\frac{VOD_{diff}}{VOD_{pd}}}{ET} \tag{17}$$

The normalization by ET demand is essential such that the metric is based on fundamental hydraulic framework and provides a strong foundation for comparisons across ecosystems and climate (Hochberg, Rockwell, et al., 2017; Novick et al., 2019), which is an improvement to the metric of isohydricity which is not normalized. Here we use ET rather than Tr for normalization because: (a) there is no readily available global daily transpiration data, (b) trying to separate transpiration from ET introduce additional uncertainties as the partitioning is highly uncertain (Li et al., 2019; Miralles et al., 2016), and most importantly (c) transpiration is highly correlated with ET spatially (Miralles et al., 2016). High R^*_{plant} (i.e., low K^*_{plant}) indicates a large leaf water potential drop during midday and suggests a weak physiological regulation of stomatal closure and xylem conductance in preventing water potential drop. R^*_{plant} is equivalent to $1/K^*_{plant}$, thus in the following sections we focus on K^*_{plant}.

2.1.3. Dryness Index Estimation

To compare different climates, a dryness index (Φ) can be defined as the ratio of potential evapotranspiration (PET) to precipitation (P) (Budyko, 1974):

$$\Phi = \frac{PET}{P} \tag{18}$$

P is obtained from the ERA-Interim Reanalysis (Dee et al., 2011). For PET, we use a recent estimate based simply on a radiation-driven method (Milly & Dunne, 2016). This method is proven to be more robust than other potential evaporation estimates (Maes et al., 2018):

$$\lambda \cdot PET = \alpha_{MD} \cdot \left(R_n - G\right) \tag{19}$$

where λ is the latent heat of vaporization (J kg^{-1}), α_{MD} is a multiplication factor, R_n and G stand for net radiation (W m^{-2}) and ground heat flux (W m^{-2}), respectively. The difference between R_n and G is equivalent to the sum of latent heat flux (LE) and sensible heat flux (H), which can also be obtained from the ERA-Interim Reanalysis (Dee et al., 2011). The dryness index is not used in the calculation of Z^*_r or K^*_{plant}, but is used to examine the variations of these proxies in relation to climate conditions.

2.1.4. K-Means Clustering

To identify the global locations where each of rooting depth and physiological regulation dominate the plant response to water stress and how these two traits coordinate globally, we use a K-means clustering (MacQueen, 1967) to categorize the magnitude of the two proxies of rooting depth $\left(Z^*_r\right)$ and physiological effects $\left(K^*_{plant}\right)$. Both the Z^*_r and K^*_{plant} are then classified into three classes each (i.e., high, medium, low), resulting in nine categories of the combined effects globally.

2.2. Proof of Concept

While it would be ideal to prove the fidelity of our methodology of deriving Z^*_r and K^*_{plant} using in-situ measurements, to the best of the authors' knowledge, there are no sites with sufficient observations of all

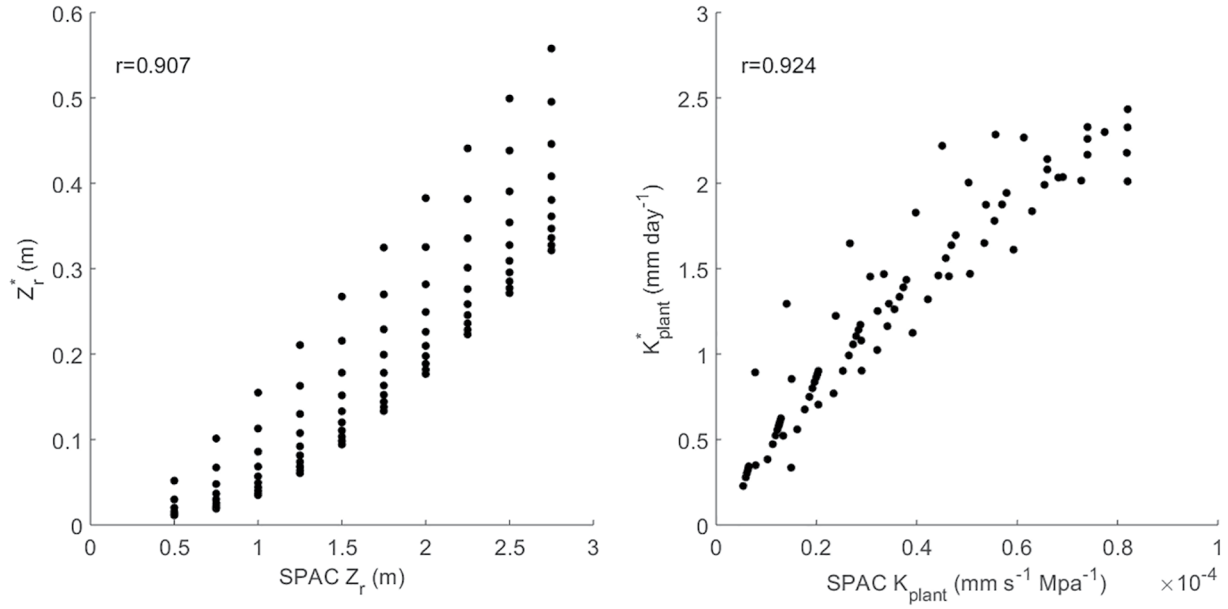

Figure 1. Scatter plot of Z_r^* and K_{plant}^* versus those prescribed/estimated Z_r and K_{plant} values in the SPAC model. The median values of Z_r^* and K_{plant}^* during the 30-day dry-down period, which we intend to represent the general condition of the 30 days, are compared to the parameters used to drive the SPAC model (each point represents one of the 100 ensemble simulations).

the associated variables, such as P, ET, ψ_s, ψ_L, Z_r, and R_{plant}, that allow us to do so. Instead, we use model simulations as a proof-of-concept of our methodology.

We use a simplified soil-plant-atmosphere continuum (SPAC) model to simulate the water supply and demand along the SPAC and the changes in water potential (see detailed description in Section S2 in the supporting information), and employ the model to prove the feasibility of our methodology. Specifically, we conduct a synthetic SPAC model experiment during a prescribed 30-day dry-down (no precipitation). The experimental simulations, each with identical forcing data, are run 100 times with 10 possible values for each of the two parameters Z_r (ranging from 0.5 to 2.5 m) and maximum hydraulic conductance k_{max} (varying from 1e^{-5} to 8e^{-5} mm s^{-1} Mpa^{-1}) prescribed independently. By running the SPAC model using the prescribed Z_r and k_{max} parameters, we obtain time-series of modeled ψ_s, ψ_L, and ET for each of the Z_r and k_{max} combinations. Then, we estimate VOD from ψ_L and plug those VOD and ET time-series into Equation 8 and 17 above to calculate the Z_r^* and K_{plant}^* (see details in Section S3 of the SI). Next, by comparing the prescribed Z_r and K_{plant} (K_{plant} is derived from the prescribed k_{max} in the SPAC, see Equations S5 and S6) in the SPAC model and the derived Z_r^* and K_{plant}^* using Equation 8 and 17, we can check the fidelity of our methods.

The comparison between the prescribed Z_r and K_{plant} and the calculated Z_r^* and K_{plant}^* reveals that our methods are effective in deriving both Z_r^* and K_{plant}^* from satellite VOD data (Figure 1), with correlation coefficients >0.9. We do not expect a perfect fit given the complexity of the water potential dynamics in response to variations in Z_r and K_{plant}, induced by nonlinearities in the system. Instead we aim to capture the emergent behavior of the system by matching (to a reasonable level) the sequencing and variations in the prescribed values of Z_r and K_{plant}. This comparison also suggests that our method is in line with the physical processes represented in the SPAC model, as it is able to trace back the wide variations in the prescribed Z_r and K_{plant}. Nevertheless, consistent with the derivation of the Z_r^* and K_{plant}^*, the assumptions behind these measures lead to differences in scale with the "true" SPAC Z_r and K_{plant}. Overall, through this model experiment, we have shown that the concept of our methodology is consistent with current plant hydraulic theory.

2.3. Data

The main data are described below, and information for ancillary data of land cover types and soil properties is detailed in S2 of the supporting information.

2.3.1. Vegetation Optical Depth

Microwave VOD product derived from the Advanced Microwave Scanning Radiometer for EOS (AMSR-E) and the Advanced Microwave Scanning Radiometer 2 (AMSR2) (Du et al., 2017) is acquired from University of Montana, with descending and ascending orbital equatorial crossings at 01:30 and 13:30 local time (http://files.ntsg.umt.edu/data/LPDR_v2/). The data provide global coverage, at daily time scale and 0.25° resolution, spanning from 2002 to 2011. These data have already been used to assess the sensitivity of VOD to leaf water potential (Momen et al., 2017) and to derive ecosystem isohydry/anisohydry (Li et al., 2017). Here, we specifically use VOD_{md} and VOD_{pd} as proxies for midday leaf water potential (ψ_L) and predawn soil water potential (ψ_s) (Konings & Gentine, 2017), respectively.

2.3.2. Reanalysis Data

Global daily climate data, including total precipitation, evapotranspiration (ET), surface sensible heat flux (H), and air temperature at 2-m height from 2002 to 2011 are obtained from the European Center for Medium-Range Weather Forecasts (ECMWF) ERA-Interim Reanalysis (Dee et al., 2011) which is available at http://apps.ecmwf.int/datasets/data/interim-full-daily/levtype=sfc/. Note that the ET data in the ERA-Interim is denoted as evaporation, which actually include evaporation from the top of canopy and the bare soil, as well as transpiration from plants. The plant physiological controls on transpiration are implicitly modeled through the use of plant functional type-based parametrizations of the stomatal closure (Dee et al., 2011; Jarvis, 1976; Viterbo & Beljaars, 1995). The data is downloaded at 0.25° resolution, after bilinear interpolation by ECMWF (Berrisford et al., 2011). The climate data are used to calculate the dryness index, to derive the Z_r^*, and to explore the relationship between plant strategies and climate conditions.

2.3.3. Enhanced Vegetation Index

Global daily two-band enhanced vegetation index (EVI) (Jiang et al., 2008) from 2002 to 2011 is obtained from University of Arizona (https://vip.arizona.edu/viplab_data_explorer.php), which is derived from MODIS, 16-day composite Vegetation Index product (MOD13A2), from Collection 4 and the Terra platform. This two-band EVI only use red and near-infrared bands, without a blue band, to derive the EVI, which can be used for sensors without a blue band and is proved to be an accurate substitute of three-band EVI (Jiang et al., 2008). The two-band EVI data are at a 0.05° climate modeling grid, and are aggregated to a 0.25° resolution to be consistent with the climate and VOD data. The EVI data are used to extract the time period of peak growing season, when the biomass variations are relatively small. The peak growing season is defined here as times when EVI is near its peak level (above the 80% percentile in each pixel).

2.3.4. Alternative Rooting Depth Estimates

Various rooting depth estimates have been previously produced (Fan et al., 2017; Kleidon, 2004; Schenk & Jackson, 2002, 2003; Schenk et al., 2009; Yang et al., 2016). Those rooting depth estimates are used to cross-validate the reasonableness of our Z_r^*, since comparison against in situ estimates is challenged by large representativeness (scaling) errors. These existing global rooting depth products are either simulated from empirical or inverse models or upscaled from point measurements. These products represent different characteristics of rooting depth, such as: the soil depth containing 95% of all roots (Schenk et al., 2009), the effective optimal depth assuming the individual plants within a grid cell behave collectively to withdraw soil water (Fan et al., 2017; Yang et al., 2016), the hydrological depth of rooting zone (in mm H_2O of plant-available water) inferred from assimilation of satellite-derived absorbed photosynthetically active radiation (Kleidon, 2004). Despite these differences in their definitions, it is expected that these products preserve some spatial similarities that allow us to evaluate our derived Z_r^*.

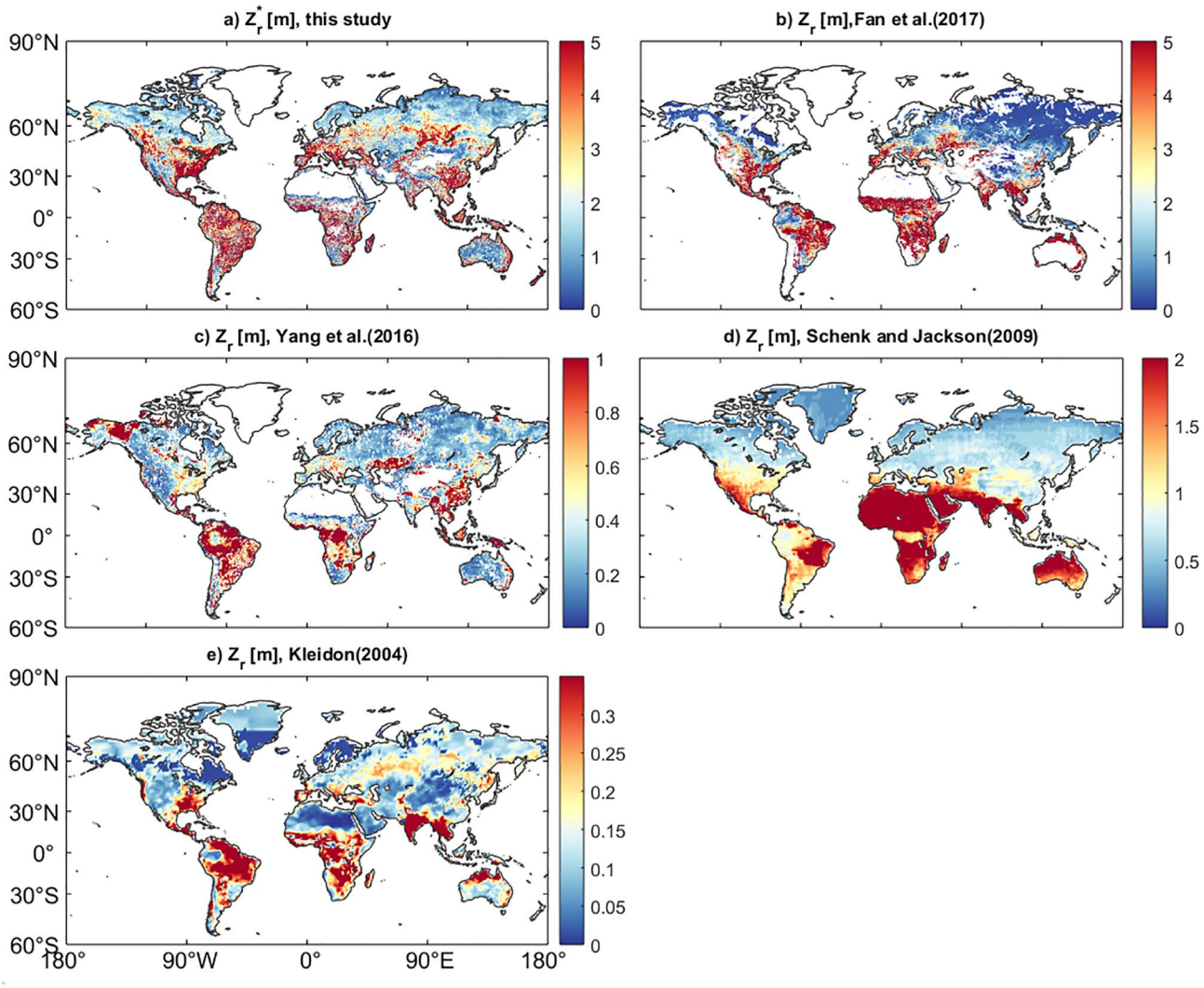

Figure 2. Spatial variations of rooting depth (Z_r) from different sources: (a) Z_r^* derived from this study assuming linear relationship between soil water content and soil water potential; (b) effective Z_r from Fan et al. (2017); (c) effective Z_r from Yang et al. (2016); (d) soil depth containing 95% of all roots (Schenk et al., 2009); and (e) hydrological depth of rooting zone in mm H_2O of plant-available water inferred from assimilation of satellite-derived absorbed photosynthetically active radiation (Kleidon, 2004).

2.3.5. In Situ Observations of Rooting Depth and Hydraulic Conductance

In-situ observations of rooting depth from Fan et al. (2017) are used to evaluate our estimated Z_r^* and other effective Z_r products. In addition, we have used K_{plant} measurements for different species from Mencuccini (2003), where measurements are collected from literature for a meta-analysis, to compare against our estimated K_{plant}^*.

3. Results

3.1. Evaluation Against In Situ Measurements

3.1.1. Evaluation of Rooting Depth Proxy

Overall, our derived Z_r^* broadly presents similar patterns with previous Z_r products (Figures 2a–2e and S2). Whether using a linear or nonlinear relationship between ψ_s and θ, the estimated Z_r^* in this work present similar global spatial patterns to previously estimated global rooting depth maps (Fan et al., 2017;

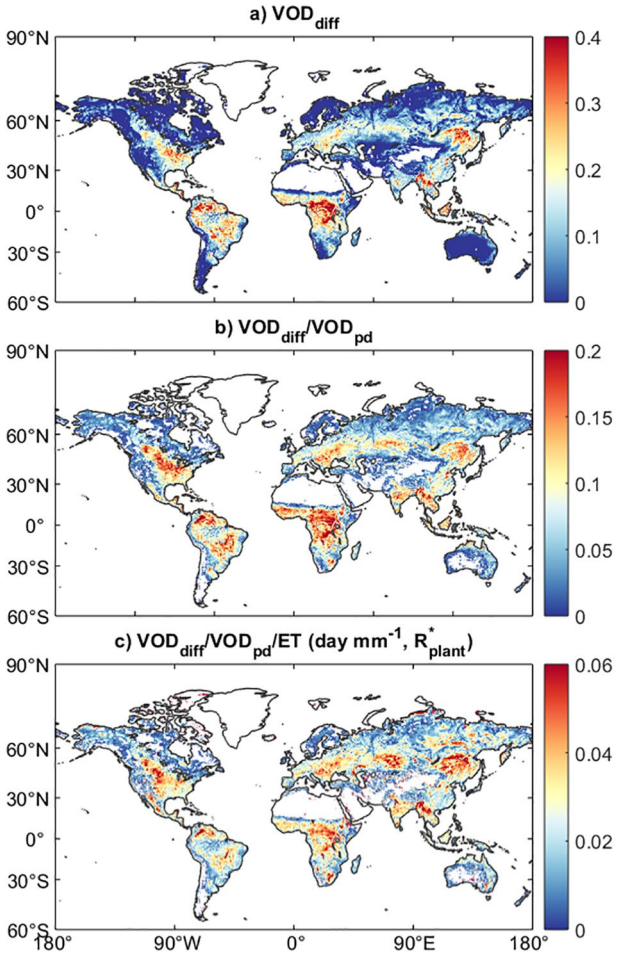

Figure 3. Spatial pattern in the difference between daily predawn VOD (VOD_{pd}) and midday VOD (VOD_{md}) (i.e., $VOD_{diff} = VOD_{pd} - VOD_{md}$): (a) long-term median VOD_{diff}; (b) long-term median VOD_{diff} normalized by VOD_{pd}; and (c) long-term median VOD_{diff} normalized by VOD_{pd} and ET.

Kleidon, 2004; Schenk et al., 2009; Yang et al., 2016). This similarity corroborates the reasonableness of the Z_r^* we derive. For better spatial coverage (as there can be data gaps when using the nonlinear version) and simplicity, we use only the linear version (Figure 2a) for the analysis in the following sections.

For further validation, we focus on the estimates of Fan et al. (2017) and Yang et al. (2016), since these are the two alternative Z_r data sets that also reflect an effective Z_r within a grid cell. Our Z_r^* has higher Spearman's rank correlation coefficient (r_s) with each of the alternative data sets ($r = 0.405$ and 0.503, respectively) than the correlation between these two data sets themselves ($r = 0.293$) (Figure S3). Though it is difficult to interpret this result with certainty, it suggests that the shared information about the true Z_r between the two alternative data sets may also be captured by our proxy. In addition, we also compare the three Z_r estimates to in situ observations of maximum rooting depth, collected in Fan et al. (2017). However, it should be noted that these measurements generally reflect only point-scale Z_r, while our Z_r^* estimates reflect the effective grid level Z_r at 0.25° resolution. Thus, very large representativeness-based differences are expected. The comparison to observations for our proxy ($r = 0.04$) is on par with that for estimates from Yang et al. (2016) (also $r = 0.04$, Figure S4). While the estimates of Fan et al. (2017) more closely match observations, this is to be expected because their product is based on those observations. Because the Fan et al. (2017) analysis is run at 30-arcsecond (<1 km) resolution rather than the 0.25° resolution of our analysis, we expect the representativeness error to be much smaller for that study. Nevertheless, these assessments confirm that our Z_r^* is comparable to other available Z_r products, yet is more directly physically constrained as described in the methodology section. The proxy also has the advantage of being consistent with the K^*_{plant} (both Z_r^* and K^*_{plant} are derived from the same instrument), and being directly informed by (microwave) observations rather than relying on a model (Figure 3).

3.1.2. Evaluation of Plant Hydraulic Conductance Proxy

Because we present the first global (median) K^*_{plant} map here, assessment of its validity is limited by the lack of both alternative gridded products and relatively low number of available in-situ measurements. Nevertheless, we compared our K^*_{plant} with the K_{plant} measurements from Mencuccini (2003), where measurements for different species have been collected for a meta-analysis of the literature (Mencuccini, 2003). Because species with very different hydraulic values often cohabit (Pangle et al., 2015), the scaling error in comparing our effective grid-scale K^*_{plant} with in situ observations is expected to be large. Overall, our estimated K^*_{plant} presents a good correlation (coefficient of determination $R^2 = 0.83$) with the measurements across plant types (conifer, shrub, broadleaf, desert sub-shrub, crop) (Figure S5), although our proxy values tend to be a bit lower. This is likely because our K^*_{plant} captures an aggregated K_{plant} reflecting species composition and diversity in plant traits within the 0.25° remote sensing pixel, whereas in-situ observations usually measure individual plants.

3.2. Global Variations in Rooting Depth and Plant Hydraulic Conductance

In the following sections, we use the Z_r^* and K^*_{plant} to delineate the variations in physiological effects and rooting depth globally. Specifically, high, medium, and low levels of K^*_{plant} correspond to strong, medium,

and weak physiological regulations, respectively. Similarly, high, medium, and low levels of Z_r^* represent deep, medium, and shallow rooting depth, respectively.

3.2.1. Spatial Variations

3.2.1.1. Rooting Depth

In our derived Z_r^* map (Figure 2a), deep roots are located in tropical regions (e.g., Amazon, equatorial Africa) and in Eastern US, as opposed to shallow rooting zones which occur in the Northern high latitudes. Further, in dry areas such as western US and inland Australia, the effective Z_r^* also tends to be shallow. While deep roots (>10 m) have been previously observed in arid climates (Schenk & Jackson, 2002), our Z_r^* in those areas is small, which is in line with the effective Z_r estimates in Yang et al. (2016). This discrepancy likely occurs because our Z_r^* reflects the effective rooting depth over a 0.25° grid unit, instead of the maximum rooting depth observed. This is probably because in arid regions the assimilated carbon is, overall, more invested into rapid growth and seeding rather than into the development of deep roots (Gentine et al., 2012).

3.2.1.2. Physiological Effects

All the three physiological metrics—VOD_{diff}, VOD_{diff}/VOD_{pd}, and $VOD_{diff}/VOD_{pd}/ET$ (i.e., proxy of R_{plant})—present relatively similar spatial patterns (Figures 3a–3c), with high values in the agricultural Midwest US, mid-latitudes of Eurasia continent, India, and Southern Asia. Most of these areas generally contain large fractions of croplands (Figure S7). Indeed, K^*_{plant} decreases with an increase in crop area percentage (Figure 4c), In croplands, physiological regulation to water stress is expected to be minimal in order to maximize photosynthesis and yield, which allows substantial drop in midday Ψ_L (Van Emmerik et al., 2016), reflecting a weak physiological regulation on stomatal closure and low xylem conductivity (Figure 4b).

In addition, Northern high latitudes where evergreen needleleaf forests (ENF), mixed forests (MF), open shrubland (OSH), and (woody) savannas are located generally exhibit lower drop in midday Ψ_L, reflecting stronger physiological regulation (higher K^*_{plant}), relative to the tropical zone (e.g., central Africa, Northern, and Southeastern Amazon) where evergreen broadleaf forests (EBF) are distributed, and Eastern US and Northeastern China where deciduous broadleaf forests (DBF) grow (Figures 3, 4 and S7). Compared to plants in Northern high latitudes, the larger drop in midday Ψ_L in EBF and DBF regions (Figure 4) may be caused by their taller canopy height (Simard et al., 2011), which induces a larger hydraulic challenge due to the water uplift over a greater distance against the effects of gravity and path length-associated viscosity resistance (Bennett et al., 2015; Giardina et al., 2018; McDowell & Allen, 2015).

3.2.2. Variations by Land Cover Type

3.2.2.1. Rooting Depth

Our estimated Z_r^* shows that forests and (woody) savannas tend to have deeper roots than other ecosystems (Figures 4a and S6). EBF, DBF, and MF have the highest effective Z_r^*. In contrast, grasslands (GR), sparse vegetation (SPA), and OSH have shallower roots. This is consistent with previous literature (Fan et al., 2017; Yang et al., 2016). The estimated Z_r^* for cropland is even higher than for woody savanna (WS) and savanna. This high value may be attributed to uncertainties in the Z_r^* associated with irrigation (Liu et al., 2015a). Irrigation, which is not accounted for in our water balance, buffers root zone moisture and thus day-to-day variations in VOD_{pd}, which would be interpreted as deeper rooting depth (because of the minimal variations in VOD_{pd}).

Differences in Z_r^* across land cover types also have an effect on their predawn Ψ_s. We find that forests such as DBF, EBF, and ENF, which typically have deeper roots, exhibit smaller variations in VOD_{pd} relative to grassland, OSH, and sparse vegetation (Figure 5). This is because the deep roots in forests can hold soil moisture and deploy hydraulic lift to minimize predawn Ψ_s variations (Caldwell et al., 1998; Ivanov et al., 2012).

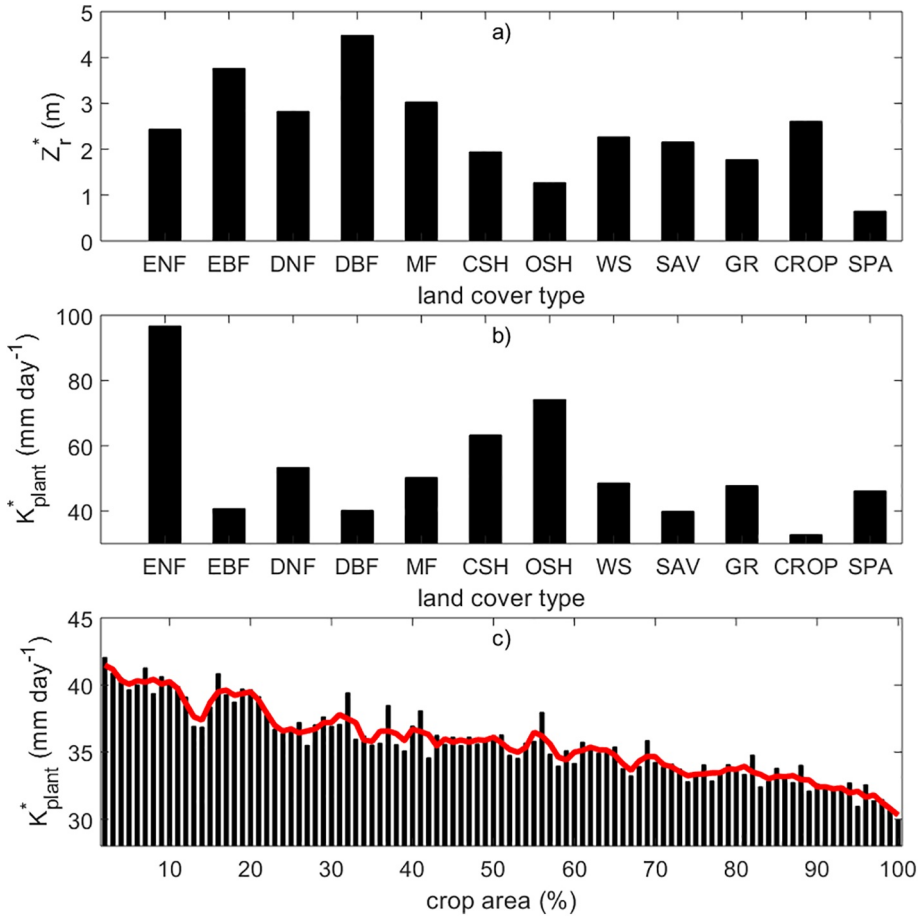

Figure 4. Variations in the proxy of rooting depth $\left(Z_r^*\right)$ and whole plant hydraulic conductance $\left(K^*_{plant}\right)$: (a) Z_r^* by land cover types; (b) K^*_{plant} by land cover types; and (c) K^*_{plant} variation with changing crop area percentage. The respective median value of Z_r^* and K^*_{plant} for each land cover type and each 1% unit crop area in all corresponding grid cells over the study period is used. The red line in (c) stands for the moving average of K^*_{plant} over 3% unit crop area percentage. In (a) and (b), ENF, evergreen needleleaf forest; EBF, evergreen broadleaf forest; DNF, deciduous needleleaf forest; DBF, deciduous broadleaf forest; MF, mixed forest; CSH, closed shrubland; OSH, open shrubland; WS, woody savanna; SAV, savanna; GR, grassland; CROP, cropland, SPA, sparse vegetation.

Another possible reason is that those deep-rooted forests grow in area less susceptible to severe water stress (Figures S7 and S8).

3.2.2.2. Physiological Effects

Our results reveal that ENF and open/closed shrublands have much stronger physiological regulations (exemplified by higher K^*_{plant}) than other forest and land cover types, with cropland presenting the lowest K^*_{plant} (Figures 4b and S6). This is in line with in-situ observations, which report ENF are often isohydric (maintaining relatively steady leaf water potential) (Klein et al., 2013; Meinzer et al., 2014) and shrubland have tight stomatal regulation (Jin et al., 2018; Mooney et al., 1983). Another reason for the larger K^*_{plant} in ENF is that they are relatively short (Simard et al., 2011) compared to other forest types, thus the total xylem hydraulic resistance for ENF is small. The low K^*_{plant} in cropland can be attributed to intervention of farming practices and plant engineering, which have been designed to maximize photosynthesis, and thus to keep stomata open. When the sap flow in crop xylem cannot sustain the demand of transpiration, it will result in large drops in midday Ψ_L compared to nighttime (Van Emmerik et al., 2016), and thus a low K^*_{plant} estimate.

VOD diurnal variations across different land cover types also reveal their differences in physiological regulation, with larger VOD_{diff}/ET reflecting weaker physiological regulation in preventing midday drop in Ψ_L.

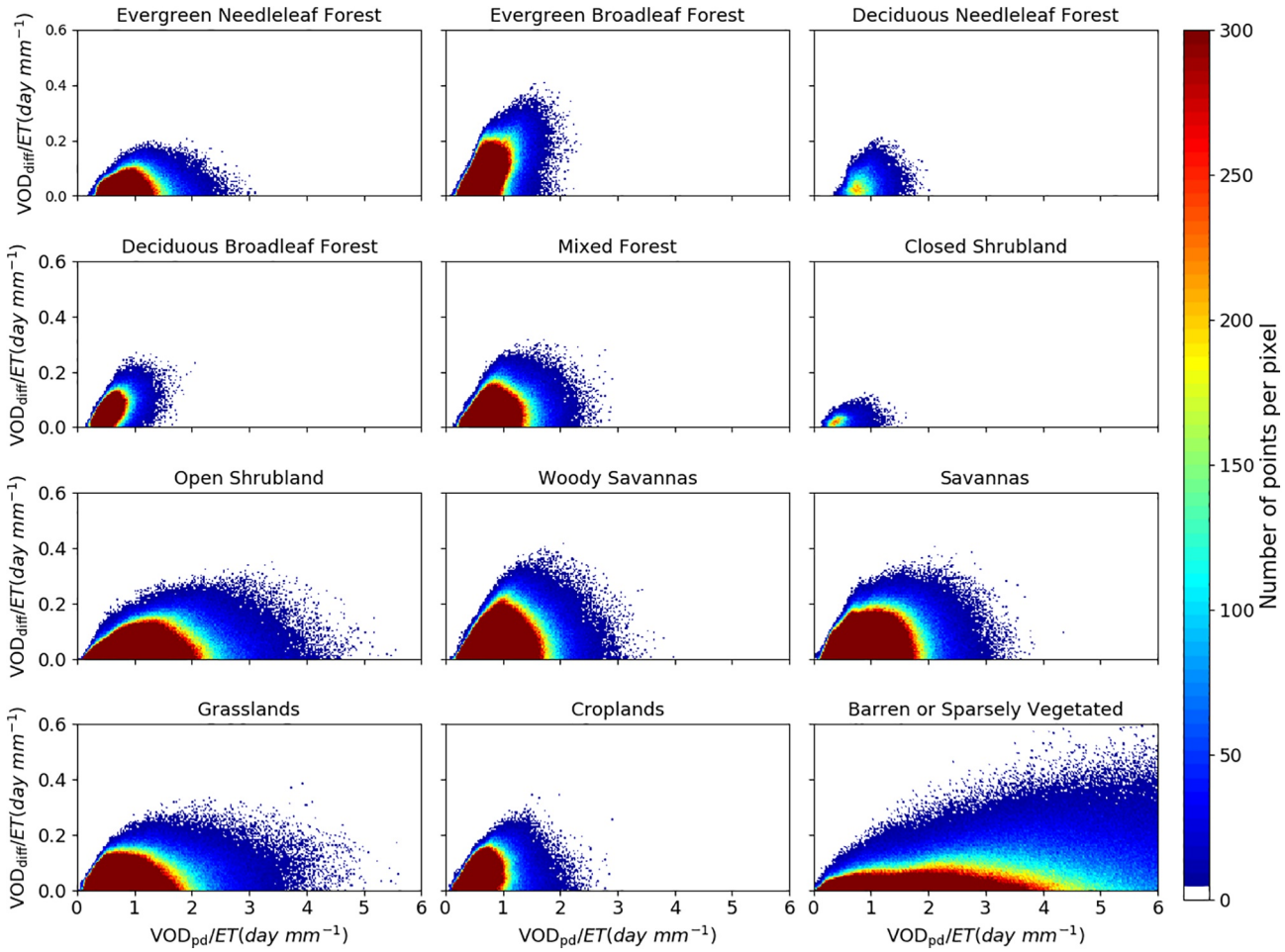

Figure 5. Scatter plot of VOD_{diff}/ET versus VOD_{pd}/ET by land cover type. VOD_{diff} stands for the difference between daily predawn VOD (VOD_{pd}) and midday VOD (VOD_{md}).

We find land cover types with taller plants and deeper roots such as EBF and WS exhibit larger variation in VOD_{diff}/ET and thus inferred $1/K^*_{plant}$ relative to shorter land cover types such as grasslands, sparse vegetation, and shrublands (Figure 5). This is consistent with previous findings that taller trees have greater physiological vulnerability due to the negative impact of pulling water to a greater height (Bennett et al., 2015; Giardina et al., 2018; McDowell & Allen, 2015), and thus resulting in larger midday $\Psi_L$drop during water stress, as a consequence of the weaker physiological regulation. Moreover, by exploring the scatterplot of the Z_r^* and K^*_{plant} by land cover type, we find similar results—forests like EBF and DBF with deeper roots usually have lower K^*_{plant} (i.e., weaker physiological regulation). On the other hand, land cover types such as OSH with more shallow roots present strong K^*_{plant} (Figure S6). In addition, we also find forests such as DBF, EBF, and ENF typically have smaller variations in VOD_{pd} relative to grassland, OSH, and sparse vegetation (Figure 5). This may be also due to the effects of hydraulic lift as elaborated in Section 3.2.2.1.

3.2.3. Variations With Climate

3.2.3.1. Rooting Depth

Z_r^* varies with water demand (PET) and supply (P), especially with their ratio (i.e., dryness index Φ = PET/P) (Figure 6a). Specifically, Z_r^* shows an abrupt increase from wet regions (e.g., Northern high latitudes) to a maximum value when PET/P is around 1 (e.g., savanna area in south-central Africa) (Figures 6a, S7, and S8), and then Z_r^* decreases rapidly until PET/P reaches approximately 2.5 (Figure 6a). Afterward, the proxy of Z_r^* exhibits a gradual decrease when the climate becomes very dry. These findings match well

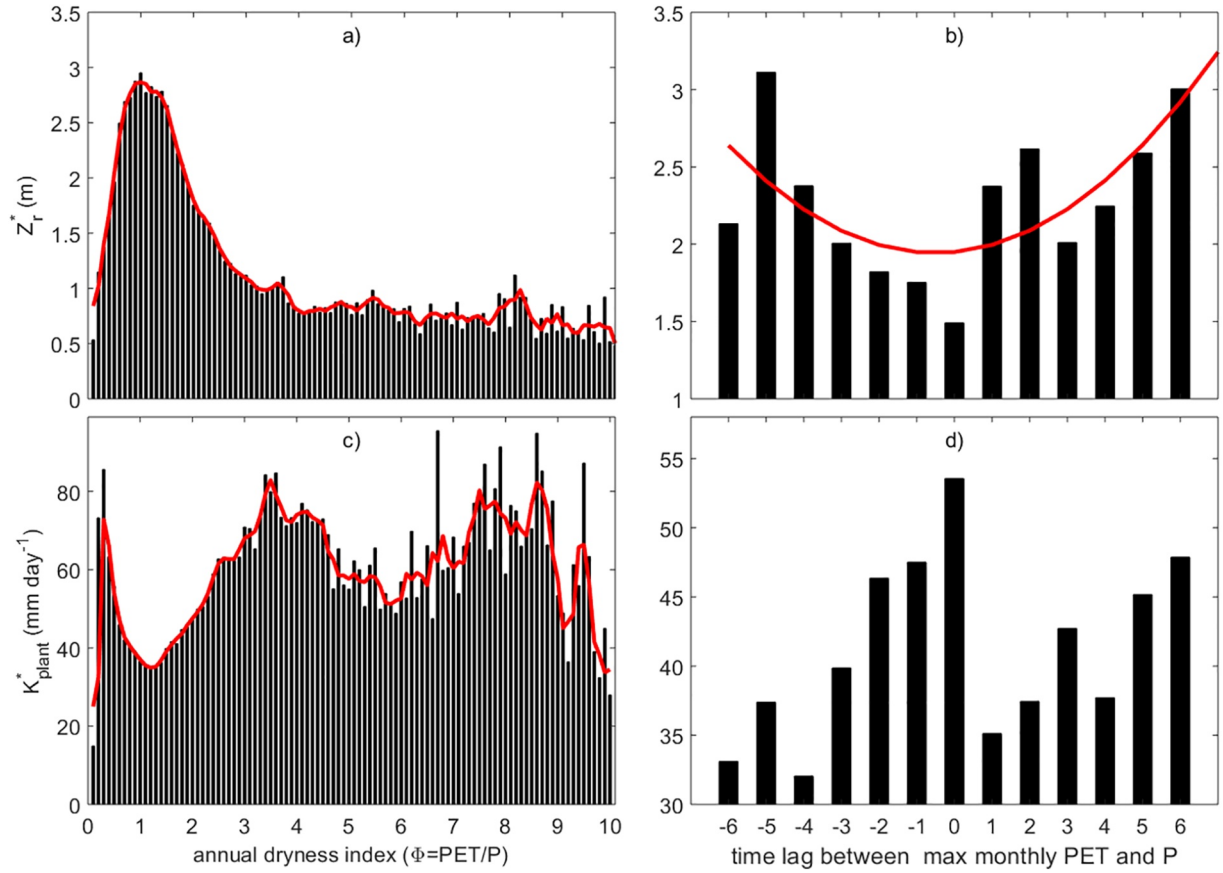

Figure 6. Relationship between the two proxies Z_r^* and K_{plant}^* and climate (dryness index Φ and synchronization of water demand and supply): (a) Z_r^* and dryness index, (b) Z_r^* and the time lag between maximum monthly PET and P. (c) K_{plant}^* and dryness index; and (d) K_{plant}^* and the time lag between maximum monthly PET and P. The respective median value of Z_r^* and K_{plant}^* for 1% unit dryness index and each time lag in all corresponding grid cells is used. The red line in (a) and (c) stands for the moving average of Z_r^* over 3 dryness index units, and that in (b) represents the best-fit quadratic function.

with a previous study (Yang et al., 2016) and are also consistent with the inverse modeling of Z_r (Gentine et al., 2012) and Z_r observations (Bhattachan et al., 2012). In humid regions (those with low PET/P), plants do not need to allocate more carbon to develop deeper roots but rather invest more carbon into aboveground biomass to maximize photosynthesis and nutrient uptake (Field et al., 1992). In transitional climate regimes (those with PET/P close to one), rooting depth becomes very deep to minimize water stress and the seasonality in moisture availability (Gentine et al., 2012). On the other hand, in very arid regions, due to carbon constraints the assimilated carbon is more invested into rapid growth and seeding rather than into development of deep roots (Gentine et al., 2012), as photosynthesis is limited by strong soil moisture reduction. Additionally, our analysis indicates that deeper roots are located in areas where water demand (i.e., PET) and water supply (i.e., P) are out-of-phase (Figure 6b), coinciding with previous studies (Gentine et al., 2012; Yang et al., 2016). In these regions, deeper roots can hold infiltrated water during the rainy season and deploy it in the dry season, reflecting an annual strategy to cope with water stress (Gentine et al., 2012; Ivanov et al., 2012).

The Z_r^* is also largely affected by climate regimes as classified with mean air temperature (T) and P. The Z_r^* increases with mean annual T (Figure 7a). Deep roots prevail in two types of regions: (1) those with precipitation of 800–1,500 mm yr^{-1} and mean temperature of 10°C–20°C; and (2) those with precipitation of 2000–3000 mm yr^{-1} and mean temperature of 25°C–30°C. An example of the former type is the deciduous broadleaf forests in the Eastern US, while evergreen broadleaf forests in the wet tropics form an example of the latter type (Figures S7 and S8). Warm temperatures facilitate plant growth, and plants may need deeper

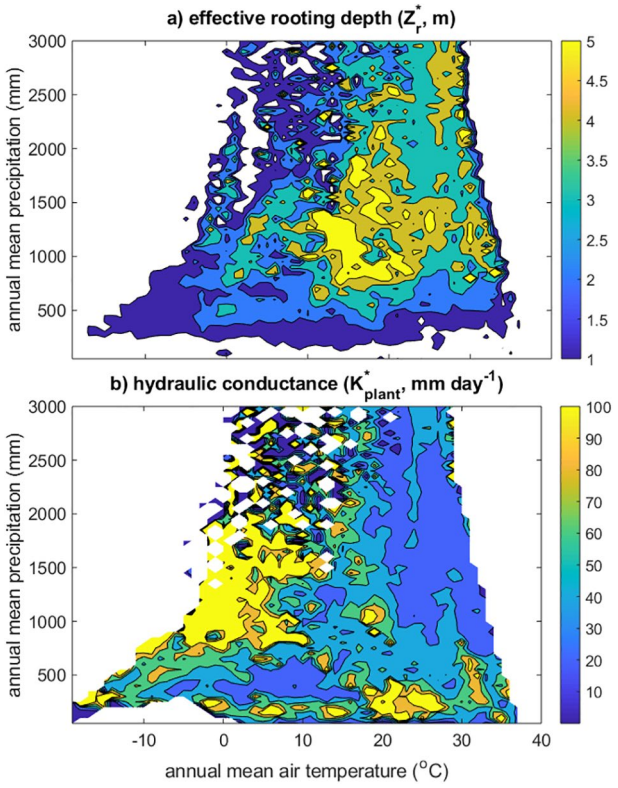

Figure 7. The relationship of the two plant strategies to water stress with annual mean air temperature and precipitation: (a) the strategy of rooting depth Z_r^*; and (b) the strategy of physiological effects exemplified by whole plant conductance K_{plant}^* (equal to $1/R_{plant}^*$).

roots to access deeper water to overcome greater hydraulic resistance and to anchor larger plants (Bennett et al., 2015; Nepstad et al., 1994).

3.2.3.2. Physiological Effects

K_{plant}^* tends to be high in areas where dryness index is either very low or high (Figure 6c). The former regions are mainly located at Northern high latitudes where PET is very low relative to precipitation (Figures S7 and S8), and the high K_{plant}^* there is associated with the short canopy height (see Section 3.2.1.2). In very dry areas such as inland Australia, the main land cover is open shrubland (Figures S7 and S8), which exhibits strong physiological regulation to survive in that dry and harsh environment (Jin et al., 2018; Mooney et al., 1983). In contrast to the Z_r^*, K_{plant}^* tends to be higher when maximum water demand (PET) synchronizes with the maximum water supply (P) season (time lag = 0). This is because most of the synchronization occurs in the Northern high latitudes (Liu et al., 2015b) where K_{plant}^* is high as discussed above.

High K_{plant}^* is more common in two main climatic zones with: (a) annual mean precipitation ranging from 700 to 2,000 mm yr^{-1} and air temperature from −10 to 10°C and (b) annual mean precipitation less than 500 mm yr^{-1} (Figure 7b). The former is located in regions such as the Northeastern US, Western, and Southeast Canada where ENF, DNF, MF, and woody savanna are distributed, and the latter covers dry areas such as inland Australia, western US, and cold area like the Arctic (Figures S7 and S9). However, areas with low K_{plant}^* occur across a range of precipitation values, spanning from arid environments (e.g., some areas of far-eastern Siberia) to very wet region (e.g., equatorial Africa) (Figures 7b and S9). This is consistent with previous findings that plant hydraulic vulnerability is independent of precipitation (Choat et al., 2012).

3.3. Dominance and Coordination of Plant Strategies Globally

K-means clustering is used to summarize the relative coordination and dominance of hydraulic (e.g., K_{plant}^* -related) and rooting depth related strategies to water stress (Figures 8 and 9). Areas with co-occurrence of medium/deep Z_r^* and medium/high K_{plant}^* suggest a coordination of the two water strategies. On the other hand, areas low in both Z_r^* and K_{plant}^* reflects a lack of presence for either strategies. In addition, regions with medium/high K_{plant}^* but low Z_r^* indicate dominance of K_{plant}^* as a water stress response strategy. Similarly, places with medium/high Z_r^* but low K_{plant}^* exhibit dominance of Z_r^* as an approach to avoid water stress.

The results show that strong physiological regulation (i.e., high K_{plant}^*) is often deployed by plants in regions where Z_r^* is low, such as the Northern high latitudes where open shrubland and (woody) savannas are distributed and over the western US grasslands (Figures 8c and S2).

The global area coverage of land where deep rooting dominates over physiological effects in response to water stress (Figure 8d) is much smaller than the regions where physiological regulations overshadow rooting strategy (Figure 8c). Nonetheless, in our results, deep rooting strategy appears to dominate over a hydraulic strategy in some croplands (Figures 8d and S7); this is likely due to the interference of irrigation as discussed in Section 3.2.2.1, which alter the water balance and the rooting depth retrieval. Another case where the derived deep Z_r^* may be unrealistic is in regions affected by groundwater flow, such as near streams. Areas next to river system such as the areas next to Amazon and Lena River have unrealistically deep Z_r^* (Figures 9 and S9), because the nighttime water potential there does not evolve much (i.e., there is not substantial drop nor detectable drydown).

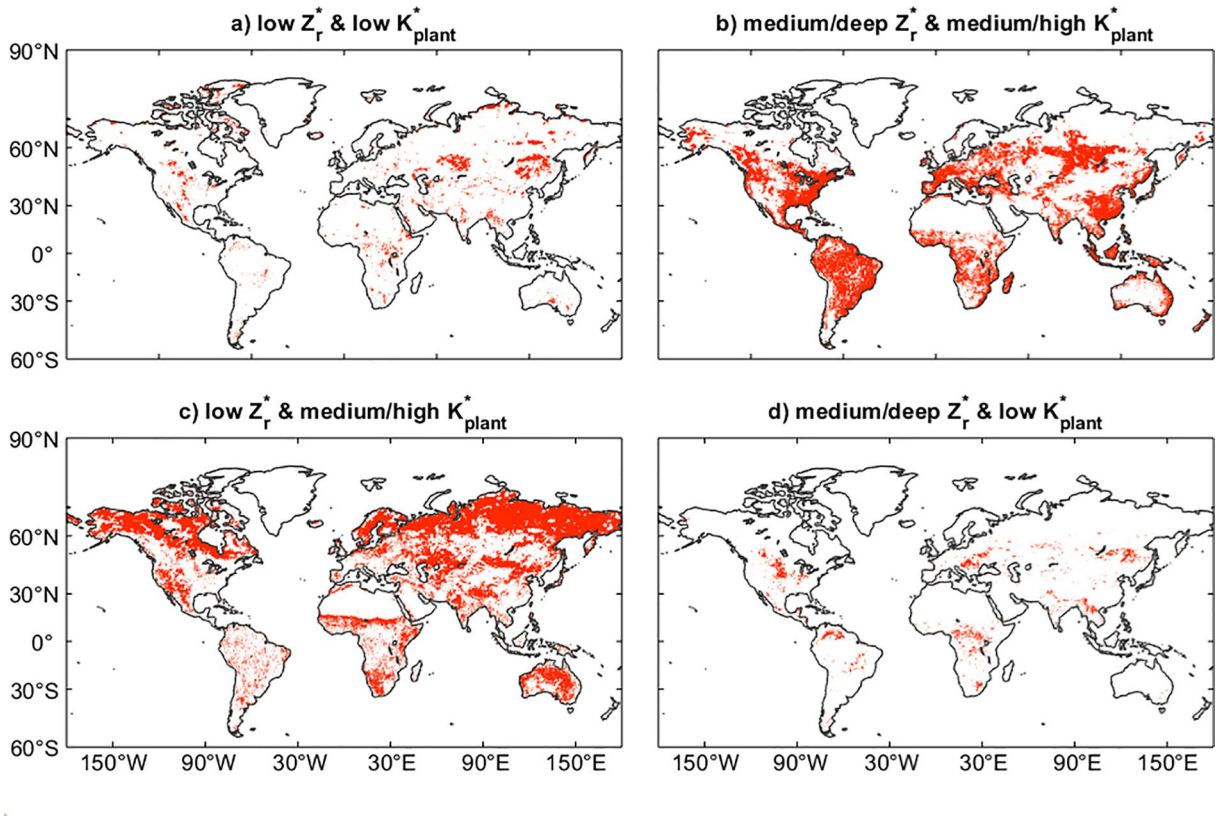

Figure 8. Spatial pattern in dominance and coordination of the two plant strategies to water stress (i.e., rooting depth Z_r^* and physiological effects exemplified by whole plant conductance K_{plant}^*): (a) both strategies are at low level; (b) both strategies coordinate with each other; (c) physiological effects dominate over rooting depth; and (d) rooting depth dominates over physiological effects. Note that all nine possible patterns are shown in this figure; some categories are grouped.

Importantly, we find the two strategies coordinate with each other across vast regions of the globe (Figures 8b and 9), such as tropical areas, Eastern US, Southeastern China, and central Siberia, which are mostly covered by forests (Figure S7). In contrast, areas with weak regulation of both strategies are located in Central Asia, Mongolia Plateau, and the Western US where grasslands are mostly distributed (Figure 8a). The absence of the two strategies in those areas suggests their potential vulnerability to future drought.

4. Discussion

4.1. Coordination of Plant Water Strategies

While there is a lack of comprehensive research on large-scale plant strategies to water stress, many studies conducted at the species level are consistent with our findings. Laboratory experiments on different clones of *Coffea canephora* indicate that deep rooting and stronger stomatal control of water use together contribute to the tolerance to water stress (Pinheiro et al., 2005). Similarly, another laboratory experiment reports that *Arabidopsis thaliana* has a coordinated regulation of stomatal and root development in response to plant water demand, with larger rooting system occurring in plants with high stomatal conductance (Hepworth et al., 2016). In addition, a study in California showed that trees can better endure drought than grasses and are also associated with stronger physiological control on stomatal closure and deeper roots (Baldocchi et al., 2004). Beyond these particular examples, here we show that coordination of different water stress strategies together is widespread.

Plants grown in Mediterranean climates, such as olive trees, have developed a series of physiological mechanisms (e.g., osmotic adjustment, antioxidant enzymes) to tolerate water stress and grow under adverse climatic conditions (Sofo et al., 2008). Further, plants in those regions show great resistance to cavitation

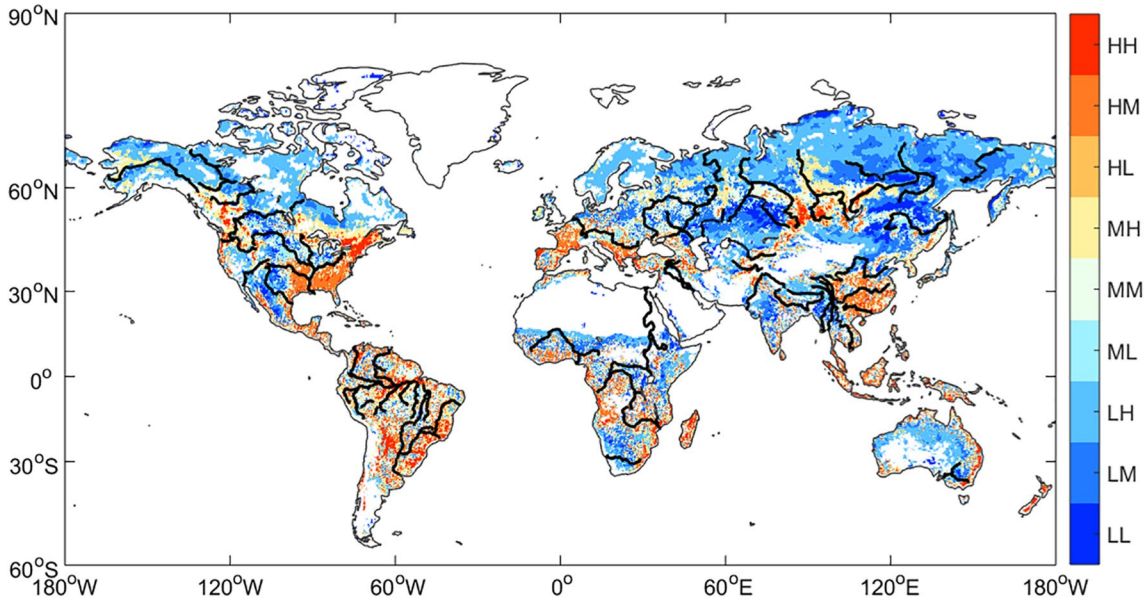

Figure 9. Joint spatial pattern of three levels of rooting depth Z_r^* and three levels of physiological effects exemplified by whole plant conductance K_{plant}^* (H, high; M, medium; L, low). The label is composed of the respective level of Z_r^* and K_{plant}^*, for instance, HM stands for high level of Z_r^* and medium level of K_{plant}^*. Note that in terms of Z_r^*, high, medium, and low levels stand for deep, medium, and shallow rooting depth, respectively. The black lines delineate the major rivers obtained from https://worldmap.harvard.edu.

(Maherali et al., 2004), trying to avoid drought-induced hydraulic dysfunction. This high level of physiological regulation in Mediterranean plants is also well captured by our analysis (Figures 8 and S9).

The Amazon has attracted a lot of attention due to its crucial role in the global carbon and hydrological cycles (Guan et al., 2015; Pan et al., 2011). Rather than investigating the two strategies together, a substantial body of literature has revealed that the Amazon forests either employ the strategies of acquiring water through deep roots (Giardina et al., 2018; Hutyra et al., 2007; Nepstad et al., 1994) or limit water losses through tight physiological regulation (Jones et al., 2014; Samanta et al., 2012). Adaptive strategies are reported to optimize plant physiology for carbon gain and diurnal evaporative demand under seasonal resource availability in the Amazon region (Anber et al., 2015; Elliott et al., 2006; Guan et al., 2015). Meanwhile, seasonal variations in leaf phenology further complicate the identification of dominant strategies. Leaf flush in the dry season and pre-flush or simultaneous leaf drop shift age composition of canopies toward abundant young leaves with higher photosynthetic efficiency, which may improve stomatal control of water loss (Reich & Borchert, 1988) and facilitate plant photosynthesis (Lopes et al., 2016; Wu et al., 2016). At the same time, stomatal closure is also reported to be employed in Central Amazon forests to cope with drought, even diurnally, at the expense of reduced photosynthesis (Fisher et al., 2006; Fontes et al., 2018; Santos et al., 2018). The interactions between rooting, leaf phenology, photosynthesis, physiology, and water stress in the Amazon region are complex and still poorly understood, requiring further research. Nonetheless, these studies converge toward our conclusion (Figures 8 and 9), indicating that the Amazon forest does not exclusively employ a single strategy but co-employ multiple strategies to optimize resources and overcome water stress.

4.2. Uncertainties and Limitations

The data selection criteria used here may introduce potential biases in our identified plant strategies to water stress. Since it is difficult to accurately identify the onset of water stress globally, we thus use all days when VOD_{pd} declines. Further, due to the year-long photosynthesis in tropical areas, the method of selecting peak EVI period (see Section 2.1) may result in discontinuous data points (Figure S1), which impair the time integrity of the dry season in our analysis and thus may cause bias in identifying plant strategies in these areas. Beyond such errors, since we only involve the peak EVI period in our analysis, this work does

not address seasonal changes in plant strategies to water stress. Such variation is another aspect of the possible plant water stress response strategies.

The relatively low temporal coverage in the VOD data in the tropics may add uncertainty to our analysis of plant strategies in that region. Due to the occurrence of rainfall, there are missing values in the VOD data in the wet tropical region (Du et al., 2017). The discontinuity of the VOD data (see Figure S1 upper middle panel) impacts the seasonal signals of leaf and soil water potential, inducing uncertainties in the examined plant strategies to water stress in the tropical region. In light of the critical role of tropical forests in global carbon and water cycling (Fauset et al., 2015; Zhao & Running, 2010), further investigations with a higher quality of observations are needed to achieve a better understanding of plant strategies in this area. Additionally, there are other sources of uncertainty, such as radio frequency interference in the measurements, cloud liquid water effects on the temperature estimates, and the prior choice of scattering albedo (Du et al., 2016; Konings, Piles, et al., 2017), in the retrieval of VOD from raw brightness temperature observations.

The inherent uncertainties in the ET data set obtained from ERA-Interim (Dee et al., 2011) may be cascaded to the K^*_{plant} as well. The quality of the latent heat flux (LE, associated with ET) in the ERA-Interim was evaluated in earlier work (Alemohammad et al., 2017) by comparing against in-situ observations from 750 FLUXNET sites globally (Baldocchi et al., 2001). The R^2 between the ERA-Interim LE and the in-situ observations is reported to be approximately 0.7, and the average bias is 3.18 W m^{-2} (Alemohammad et al., 2017), reflecting a reasonably good quality of the ET in the ERA-Interim despite its inherent uncertainties. Additionally, it should be noted that the ERA-Interim ET also has assumptions about rooting depth (which varies by plant functional type) and about the response of ET to water stress, a concept that varies with K_{plant}. Nevertheless, the high correlations between FLUXNET sites and ERA-Interim latent heat suggest that these implicit assumptions, when combined with the rest of the ERA-Interim model, have a relatively small effect on the overall data set accuracy.

Internal water storage capacity is not explicitly explored in this work, although it is indirectly embedded in the integrated physiological effects proxy $\left(K^*_{plant}\right)$ we analyze. Water storage in plants is an adaption that helps plants avoid hydraulic failure and withstand water stress (Holbrook, 1995). Reliance on stored water increases with tree size. For example, stored water in the xylem of Douglas-fir accounted for 20%–25% of total daily water use in 60-m trees but only 7% in 15-m trees (Phillips et al., 2003). Further, the stored water will delay drought-induced cavitation and help plants maintain the integrity of the plant water transport system, buffer daily fluctuations in xylem pressure, and survive drought (Epila et al., 2017). Nevertheless, currently available observations and tools are not sufficient to examine these issues at global scale.

Uncertainties in the Z_r^* we derive here largely arise from assumptions pertaining to the relationship between VOD, θ, Ψ_s, and Ψ_L, the pedotransfer functions as well as the inherent uncertainties cascaded from the climate and soil data. Furthermore, the K^*_{plant} of physiological effects derived from VOD here does not encompass a full suite of plant physiological strategies to water stress. Ideally, these assumptions would be explicitly validated at the site scale. However, to the best of the authors' knowledge, no sites are available with sufficient observations and trait measurements to fully test the method used here. This points to a need for additional site observations integrating plant hydraulics and hydrological observations, as further discussed in the section below.

4.3. The Need for an Integrated Observation Network

Field experimentalists design experiments and measure variables of interest based on their respective research needs. For example, the plant physiology community usually measures physiology-related traits such as leaf water potential (Ψ_L), soil water potential (Ψ_s), transpiration (T_r), stomatal conductance (g_s), plant hydraulic conductance (K_{plant}), but may omit rooting depths at the same time (Cinnirella et al., 2002; Kattge et al., 2011; Martinez-Vilalta et al., 2014; Mencuccini, 2003). Similarly, the eddy covariance community usually measures meteorology and fluxes (e.g., precipitation, latent heat flux) and biogeochemical variables (e.g., net ecosystem exchange, ecosystem respiration) but usually do not observe the rooting depth (Pastorello et al., 2020). Likewise, plant morphology researchers usually observe structural parameters of plants

and plant traits such as rooting depth (Z_r), root biomass distribution and leaf size and number, but may not measure plant hydraulic traits or time series of hydrological quantities (e.g., soil moisture, transpiration) (Fan et al., 2017; Kattge et al., 2011; Schenk & Jackson, 2002, 2003; Schenk et al., 2009). As a result, to the author's best knowledge, no field sites exist that combine the variables of interest (P, T_r, Ψ_{L_md}, Ψ_{L_pd}, Ψ_s, K_{plant}, Z_r) for this study and that would allow us to validate our methodology of deriving Z_r and K_{plant} from VOD.

The lack of comprehensive in situ observations to test models and satellite-derived estimates such as those presented here underscores the needs for a coordination of efforts from different research communities. Aligning with this goal, a dialogue between different communities of field experimentalists and the microwave remote sensing community has started to close this gap, as evidenced in the series of workshops on "Sensing Forest Water Dynamics from Space: Toward Predicting the Earth System Response to Droughts." These and other efforts should pave the road to a more integrated observation network.

Despite all these caveats, this work presents the first global assessment of coordination between plant strategies to water stress in relation to climate and land cover type. Incorporating these findings into Earth System models could improve drought prediction and impact assessment.

5. Conclusion

Using daily microwave vegetation optical depth (VOD) from AMSR-E and AMSR-2 and the water mass balance equation, this work conducts the first global estimate of the coordination of plant strategies (mainly deep rooting and strong physiological regulation) to water stress, and also examines their variations with climate and land cover type. We mainly find strong physiological regulation appears to be the dominant strategy in Northern high latitudes, whereas it couples with deep rooting in the tropics, Eastern US, and Southeastern China. Meanwhile, some grassland areas in the Western US, Central Asia, Northeastern China, and Mongolia Plateau do not possess either of these strategies, suggesting their potential vulnerability to future droughts.

Our work has three important implications. First, we collectively examine both the morphological and physiological plant strategies to water stress, depicting the first (to our knowledge) global assessment of dominance and coordination of these water stress strategies. It is consistent with past research ranging from laboratory experiments to site level field survey, and to modeling work in the community of hydrology and plant physiology, suggesting the potential merits of integrating the efforts from these two communities for a better understanding of plant strategies. Second, our findings can inform current Earth system models that typically do not include plant hydraulics. This is critical in a drought-intensifying context for improving prediction of drought occurrence and assessment of drought impacts as well as carbon dynamics due to the inherent coupling of water and carbon. As we have demonstrated in many regions, physiological regulations and deep rooting may not be coordinated (Figures 8c–8d), so models with only rooting depth adjustment could not well represent plant responses in those regions. By improving those predictions, it would help inform policy makers in mitigating drought-induced social and ecological impacts. Third, this work showcases the potential of the microwave VOD product to detect variations in soil to leaf water potentials, and thus for monitoring plant hydraulics. Our estimates of global rooting depth proxy and plant hydraulic resistance proxy are freely available at GitHub (https://github.com/yalingliu-cu/plant-strategies).

Data Availability Statement

All data used in this work are available through these in-text references: Dee et al. (2011), Du et al. (2017), Fan et al. (2017), Jiang et al. (2008), Kattge et al. (2011), Kleidon (2004), Rodell et al. (2004), Schenk et al. (2009), Yang et al. (2016), and NASA's Land Processes Distributed Active Archive Center (https://e4ftl01.cr.usgs.gov/MOTA/MCD12C1.006/) (see Section 2.3 and S4 in the supporting information).

Acknowledgments
This research is supported by the Modeling, Analysis, Predictions and Projections (MAPP) program of NOAA NA17OAR4310127 and NASA NN-H17ZDA00IN-THP to P.G. and A.G.K., A.G.K was also partially supported by NASA Terrestrial Ecology award 80NSSC18K0715 through the New Investigator Program and by the NASA award 16-CARBON16-0130.

References

Alemohammad, S. H., Fang, B., Konings, A. G., Aires, F., Green, J. K., Kolassa, J., et al. (2017). Water, Energy, and Carbon with Artificial Neural Networks (WECANN): A statistically-based estimate of global surface turbulent fluxes and gross primary productivity using solar-induced fluorescence. *Biogeosciences*, *14*(18), 4101–4124. https://doi.org/10.5194/bg-14-4101-2017

Allen, C. D., Macalady, A. K., Chenchouni, H., Bachelet, D., McDowell, N., Vennetier, M., et al. (2010). A global overview of drought and heat-induced tree mortality reveals emerging climate change risks for forests. *Forest Ecology and Management*, *259*(4), 660–684. https://doi.org/10.1016/j.foreco.2009.09.001

Anber, U., Gentine, P., Wang, S., & Sobel, A. H. (2015). Fog and rain in the Amazon. *Proceedings of the National Academy of Sciences*, *112*(37), 11473–11477. https://doi.org/10.1073/pnas.1505077112

Anderegg, W. R., Konings, A. G., Trugman, A. T., Yu, K., Bowling, D. R., Gabbitas, R., et al. (2018). Hydraulic diversity of forests regulates ecosystem resilience during drought. *Nature*, *561*(7724), 538–541. https://doi.org/10.1038/s41586-018-0539-7

Aroca, R. (2012). *Plant responses to drought stress, from morphological to molecular features*. Springer-Verlag.

Baldocchi, D., Falge, E., Gu, L., Olson, R., Hollinger, D., Running, S., et al. (2001). FLUXNET: A new tool to study the temporal and spatial variability of ecosystem-scale carbon dioxide, water vapor, and energy flux densities. *Bulletin of the American Meteorological Society*, *82*(11), 2415–2434. https://doi.org/10.1175/1520-0477(2001)082<2415:fantts>2.3.co;2

Baldocchi, D. D., Xu, L., & Kiang, N. (2004). How plant functional-type, weather, seasonal drought, and soil physical properties alter water and energy fluxes of an oak–grass savanna and an annual grassland. *Agricultural and Forest Meteorology*, *123*(1–2), 13–39. https://doi.org/10.1016/j.agrformet.2003.11.006

Ball, J. T., Woodrow, I. E., & Berry, J. A. (1987). A model predicting stomatal conductance and its contribution to the control of photosynthesis under different environmental conditions, In Progress in photosynthesis research (pp. 221–224). Springer. https://doi.org/10.1007/978-94-017-0519-6_48

Bartlett, M. K., Klein, T., Jansen, S., Choat, B., & Sack, L. (2016). The correlations and sequence of plant stomatal, hydraulic, and wilting responses to drought. *Proceedings of the National Academy of Sciences*, *113*(46), 13098–13103. https://doi.org/10.1073/pnas.1604088113

Bennett, A. C., McDowell, N. G., Allen, C. D., & Anderson-Teixeira, K. J. (2015). Larger trees suffer most during drought in forests worldwide. *Nature Plants*, *1*(10), 15139. https://doi.org/10.1038/nplants.2015.139

Berrisford, P., Dee, D., Poli, P., Brugge, R., Fielding, K., Fuentes, M., et al. (2011). *The ERA-Interim archive, version 2.0*.

Bhattachan, A., Tatlhego, M., Dintwe, K., O'Donnell, F., Caylor, K. K., Okin, G. S., et al. (2012). Evaluating ecohydrological theories of woody root distribution in the Kalahari. *PLoS One*, *7*(3), e33996. https://doi.org/10.1371/journal.pone.0033996

Blum, A. (2005). Drought resistance, water-use efficiency, and yield potential—Are they compatible, dissonant, or mutually exclusive? *Australian Journal of Agricultural Research*, *56*(11), 1159–1168. https://doi.org/10.1071/ar05069

Bonan, G., Williams, M., Fisher, R., & Oleson, K. (2014). Modeling stomatal conductance in the earth system: Linking leaf water-use efficiency and water transport along the soil–plant–atmosphere continuum. *Geoscientific Model Development*, *7*(5), 2193–2222. https://doi.org/10.5194/gmd-7-2193-2014

Bréda, N., Huc, R., Granier, A., & Dreyer, E. (2006). Temperate forest trees and stands under severe drought: A review of ecophysiological responses, adaptation processes and long-term consequences. *Annals of Forest Science*, *63*(6), 625–644. https://doi.org/10.1051/forest:2006042

Budyko, M. (1974). *Climate and life* (p. 508). Academic Press.

Caldwell, M. M., Dawson, T. E., & Richards, J. H. (1998). Hydraulic lift: Consequences of water efflux from the roots of plants. *Oecologia*, *113*(2), 151–161. https://doi.org/10.1007/s004420050363

Choat, B., Brodribb, T. J., Brodersen, C. R., Duursma, R. A., López, R., & Medlyn, B. E. (2018). Triggers of tree mortality under drought. *Nature*, *558*(7711), 531–539. https://doi.org/10.1038/s41586-018-0240-x

Choat, B., Jansen, S., Brodribb, T. J., Cochard, H., Delzon, S., Bhaskar, R., et al. (2012). Global convergence in the vulnerability of forests to drought. *Nature*, *491*(7426), 752–755. https://doi.org/10.1038/nature11688

Christoffersen, B. O., Gloor, E., Fauset, S., Fyllas, N. M., Galbraith, D. R., Baker, T. R., et al. (2016). Linking hydraulic traits to tropical forest function in a size-structured and trait-driven model (TFS v. 1-Hydro). *Geoscientific Model Development*, *9*, 4227–4255. https://doi.org/10.5194/gmd-9-4227-2016

Cinnirella, S., Magnani, F., Saracino, A., & Borghetti, M. (2002). Response of a mature Pinus laricio plantation to a three-year restriction of water supply: Structural and functional acclimation to drought. *Tree Physiology*, *22*, 21–30. https://doi.org/10.1093/treephys/22.1.21

Dee, D. P., Uppala, S. M., Simmons, A., Berrisford, P., Poli, P., Kobayashi, S., et al. (2011). The ERA-Interim reanalysis: Configuration and performance of the data assimilation system. *Quarterly Journal of the Royal Meteorological Society*, *137*(656), 553–597. https://doi.org/10.1002/qj.828

Du, J., Kimball, J. S., & Jones, L. A. (2016). Passive microwave remote sensing of soil moisture based on dynamic vegetation scattering properties for AMSR-E. *IEEE Transactions on Geoscience and Remote Sensing*, *54*(1), 597–608. https://doi.org/10.1109/tgrs.2015.2462758

Du, J., Kimball, J. S., Jones, L. A., Kim, Y., Glassy, J. M., & Watts, J. D. (2017). A global satellite environmental data record derived from AMSR-E and AMSR2 microwave Earth observations. *Earth System Science Data*, *9*, 791–808. https://doi.org/10.5194/essd-9-791-2017

Elliott, S., Baker, P. J., & Borchert, R. (2006). Leaf flushing during the dry season: The paradox of Asian monsoon forests. *Global Ecology and Biogeography*, *15*(3), 248–257. https://doi.org/10.1111/j.1466-8238.2006.00213.x

Epila, J., Baerdemaeker, De, N. J., Vergeynst, L. L., Maes, W. H., Beeckman, H., & Steppe, K. (2017). Capacitive water release and internal leaf water relocation delay drought-induced cavitation in African Maesopsis eminii. *Tree Physiology*, *37*(4), 481–490.

Fan, Y., Miguez-Macho, G., Jobbágy, E. G., Jackson, R. B., & Otero-Casal, C. (2017). Hydrologic regulation of plant rooting depth. *Proceedings of the National Academy of Sciences*, *114*(40), 10572–10577. https://doi.org/10.1073/pnas.1712381114

Farooq, M., Wahid, A., Kobayashi, N., Fujita, D., & Basra, S. (2009). Plant drought stress: Effects, mechanisms and management. In Sustainable agriculture (pp. 153–188). Springer. https://doi.org/10.1007/978-90-481-2666-8_12

Fauset, S., Johnson, M. O., Gloor, M., Baker, T. R., Monteagudo, A., Brienen, R. J., et al. (2015). Hyperdominance in Amazonian forest carbon cycling. *Nature Communications*, *6*, 6857.

Field, C. B., Chapin, F. S., III, Matson, P. A., & Mooney, H. A. (1992). Responses of terrestrial ecosystems to the changing atmosphere: A resource-based approach. *Annual Review of Ecology and Systematics*, *23*(1), 201–235. https://doi.org/10.1146/annurev.es.23.110192.001221

Fisher, R. A., Williams, M., Vale, Do, R. L., Costa, Da, A. L., & Meir, P. (2006). Evidence from Amazonian forests is consistent with isohydric control of leaf water potential. *Plant, Cell and Environment*, *29*(2), 151–165. https://doi.org/10.1111/j.1365-3040.2005.01407.x

Fontes, C. G., Dawson, T. E., Jardine, K., McDowell, N., Gimenez, B. O., Anderegg, L., et al. (2018). Dry and hot: The hydraulic consequences of a climate change–type drought for Amazonian trees. *Philosophical Transactions of the Royal Society B: Biological Sciences*, *373*(1760), 20180209. https://doi.org/10.1098/rstb.2018.0209

Gentine, P., D'Odorico, P., Lintner, B. R., Sivandran, G., & Salvucci, G. (2012). Interdependence of climate, soil, and vegetation as constrained by the Budyko curve. *Geophysical Research Letters*, *39*(19), L19404. https://doi.org/10.1029/2012gl053492

Giardina, F., Konings, A. G., Kennedy, D., Alemohammad, S. H., Oliveira, R. S., Uriarte, M., & Gentine, P. (2018). Tall Amazonian forests are less sensitive to precipitation variability. *Nature Geoscience*, *11*, 405–409.

Gowda, V. R., Henry, A., Yamauchi, A., Shashidhar, H., & Serraj, R. (2011). Root biology and genetic improvement for drought avoidance in rice. *Field Crops Research*, *122*(1), 1–13. https://doi.org/10.1016/j.fcr.2011.03.001

Green, J. K., Konings, A. G., Alemohammad, S. H., Berry, J., Entekhabi, D., Kolassa, J., et al. (2017). Regionally strong feedbacks between the atmosphere and terrestrial biosphere. *Nature Geoscience*, *10*(6), 410–414. https://doi.org/10.1038/ngeo2957

Green, J. K., Seneviratne, S. I., Berg, A. M., Findell, K. L., Hagemann, S., Lawrence, D. M., & Gentine, P. (2019). Large influence of soil moisture on long-term terrestrial carbon uptake. *Nature*, *565*(7740), 476–479. https://doi.org/10.1038/s41586-018-0848-x

Guan, K., Pan, M., Li, H., Wolf, A., Wu, J., Medvigy, D., et al. (2015). Photosynthetic seasonality of global tropical forests constrained by hydroclimate. *Nature Geoscience*, *8*(4), 284–289. https://doi.org/10.1038/ngeo2382

Hepworth, C., Turner, C., Landim, M. G., Cameron, D., & Gray, J. E. (2016). Balancing water uptake and loss through the coordinated regulation of stomatal and root development. *PLoS One*, *11*(6), e0156930. https://doi.org/10.1371/journal.pone.0156930

Hochberg, U., Rockwell, F. E., Holbrook, N. M., & Cochard, H. (2017a). Iso/anisohydry: A plant–environment interaction rather than a simple hydraulic trait. *Trends in Plant Science*, *23*(2), 112–120. https://doi.org/10.1016/j.tplants.2017.11.002

Hochberg, U., Windt, C. W., Ponomarenko, A., Zhang, Y.-J., Gersony, J., Rockwell, F. E., & Holbrook, N. M. (2017b). Stomatal closure, basal leaf embolism and shedding protect the hydraulic integrity of grape stems, *Plant Physiology*, *174*(2), 764–775. https://doi.org/10.1104/pp.16.01816

Holbrook, N. M. (1995). Stem water storage, In Plant stems (pp. 151–174). Elsevier. https://doi.org/10.1016/b978-012276460-8/50009-6

Hubau, W., Lewis, S. L., Phillips, O. L., Affum-Baffoe, K., Beeckman, H., Cuní-Sanchez, A., et al. (2020). Asynchronous carbon sink saturation in African and Amazonian tropical forests. *Nature*, *579*(7797), 80–87.

Hutyra, L. R., Munger, J. W., Saleska, S. R., Gottlieb, E., Daube, B. C., Dunn, A. L., et al. (2007). Seasonal controls on the exchange of carbon and water in an Amazonian rain forest. *Journal of Geophysical Research: Biogeosciences*, *112*(G3), G03008. https://doi.org/10.1029/2006jg000365

Ivanov, V. Y., Hutyra, L. R., Wofsy, S. C., Munger, J. W., Saleska, S. R., Oliveira, R. C., & Camargo, P. B. (2012). Root niche separation can explain avoidance of seasonal drought stress and vulnerability of overstory trees to extended drought in a mature Amazonian forest. *Water Resources Research*, *48*(12). https://doi.org/10.1029/2012wr011972

Jackson, R., Canadell, J., Ehleringer, J. R., Mooney, H., Sala, O., & Schulze, E. (1996). A global analysis of root distributions for terrestrial biomes. *Oecologia*, *108*(3), 389–411. https://doi.org/10.1007/bf00333714

Jarvis, P. (1976). The interpretation of the variations in leaf water potential and stomatal conductance found in canopies in the field. *Philosophical Transactions of the Royal Society of London. B, Biological Sciences*, *273*(927), 593–610. https://doi.org/10.1098/rstb.1976.0035

Jiang, Z., Huete, A. R., Didan, K., & Miura, T. (2008). Development of a two-band enhanced vegetation index without a blue band. *Remote Sensing of Environment*, *112*(10), 3833–3845. https://doi.org/10.1016/j.rse.2008.06.006

Jin, M., Guo, M., Yue, G., Li, J., Yang, S., Zhao, P., & Su, Y. (2018). An unusual strategy of stomatal control in the desert shrub Ammopiptanthus mongolicus. *Plant Physiology and Biochemistry*, *125*, 13–26. https://doi.org/10.1016/j.plaphy.2018.01.017

Jones, M. O., Kimball, J. S., & Nemani, R. R. (2014). Asynchronous Amazon forest canopy phenology indicates adaptation to both water and light availability. *Environmental Research Letters*, *9*(12), 124021. https://doi.org/10.1088/1748-9326/9/12/124021

Kattge, J., Diaz, S., Lavorel, S., Prentice, I. C., Leadley, P., Bönisch, G., et al. (2011). TRY–A global database of plant traits. *Global Change Biology*, *17*(9), 2905–2935.

Kennedy, D., Swenson, S., Oleson, K. W., Lawrence, D. M., Fisher, R., Lola da Costa, A. C., & Gentine, P. (2019). Implementing plant hydraulics in the Community Land Model, version 5. *Journal of Advances in Modeling Earth Systems*, *11*(2), 485–513. https://doi.org/10.1029/2018ms001500

Kleidon, A. (2004). Global datasets of rooting zone depth inferred from inverse methods. *Journal of Climate*, *17*(13), 2714–2722. https://doi.org/10.1175/1520-0442(2004)017<2714:gdorzd>2.0.co;2

Klein, T., Shpringer, I., Fikler, B., Elbaz, G., Cohen, S., & Yakir, D. (2013). Relationships between stomatal regulation, water-use, and water-use efficiency of two coexisting key Mediterranean tree species. *Forest Ecology and Management*, *302*, 34–42. https://doi.org/10.1016/j.foreco.2013.03.044

Konings, A. G., & Gentine, P. (2017). Global variations in ecosystem-scale isohydricity. *Global Change Biology*, *23*(2), 891–905. https://doi.org/10.1111/gcb.13389

Konings, A. G., Piles, M., Das, N., & Entekhabi, D. (2017). L-band vegetation optical depth and effective scattering albedo estimation from SMAP. *Remote Sensing of Environment*, *198*, 460–470. https://doi.org/10.1016/j.rse.2017.06.037

Konings, A. G., Williams, A., & Gentine, P. (2017). Sensitivity of grassland productivity to aridity controlled by stomatal and xylem regulation. *Nature Geoscience*, *10*(4), 284–288. https://doi.org/10.1038/ngeo2903

Lambers, H., & Oliveira, R. S. (2019). Plant water relations. In Plant physiological ecology. (pp. 187–263). Springer. https://doi.org/10.1007/978-3-030-29639-1_5

Lewis, S. L. (2006). Tropical forests and the changing earth system. *Philosophical Transactions of the Royal Society of London B Biological Sciences*, *361*(1465), 195–210. https://doi.org/10.1098/rstb.2005.1711

Li, X., Gentine, P., Lin, C., Zhou, S., Sun, Z., Zheng, Y., et al. (2019). A simple and objective method to partition evapotranspiration into transpiration and evaporation at eddy-covariance sites. *Agricultural and Forest Meteorology*, *265*, 171–182. https://doi.org/10.1016/j.agrformet.2018.11.017

Li, Y., Guan, K., Gentine, P., Konings, A. G., Meinzer, F. C., Kimball, J. S., et al. (2017). Estimating global ecosystem isohydry/anisohydry using active and passive microwave satellite data. *Journal of Geophysical Research: Biogeosciences*, *122*(12), 3306–3321. https://doi.org/10.1002/2017jg003958

Lipiec, J., Doussan, C., Nosalewicz, A., & Kondracka, K. (2013). Effect of drought and heat stresses on plant growth and yield: A review. *International Agrophysics*, *27*(4), 463–477. https://doi.org/10.2478/intag-2013-0017

Liu, Y., Pan, Z., Zhuang, Q., Miralles, D. G., Teuling, A. J., Zhang, T., et al. (2015a). Agriculture intensifies soil moisture decline in Northern China. *Scientific Reports*, *5*, 11261. https://doi.org/10.1038/srep11261

Liu, Y., Zhuang, Q., Miralles, D., Pan, Z., Kicklighter, D., Zhu, Q., et al. (2015b). Evapotranspiration in Northern Eurasia: Impact of forcing uncertainties on terrestrial ecosystem model estimates. *Journal of Geophysical Research: Atmospheres*, *120*(7), 2647–2660. https://doi.org/10.1002/2014jd022531

Lopes, A. P., Nelson, B. W., Wu, J., Alencastro Graça, de, P. M. L., Tavares, J. V., Prohaska, N., et al. (2016). Leaf flush drives dry season green-up of the Central Amazon. *Remote Sensing of Environment*, *182*, 90–98. https://doi.org/10.1016/j.rse.2016.05.009

Lyon, J. G., Trimble, S. W., Ward, A. D., & Burckhard, S. R. (2015). *Environmental hydrology*. CRC Press.

Mackay, D. S., Roberts, D. E., Ewers, B. E., Sperry, J. S., McDowell, N. G., & Pockman, W. T. (2015). Interdependence of chronic hydraulic dysfunction and canopy processes can improve integrated models of tree response to drought. *Water Resources Research*, *51*(8), 6156–6176. https://doi.org/10.1002/2015wr017244

MacQueen, J. (1967). Some methods for classification and analysis of multivariate observations. Paper presented at Proceedings of the fifth Berkeley symposium on mathematical statistics and probability, Oakland, CA, USA.

Maes, W., Gentine, P., Verhoest, N., & Gonzalez Miralles, D. (2018). Potential evaporation at eddy-covariance sites across the globe. *Hydrology and Earth System Sciences*, *23*(2), 925–948.

Maherali, H., Pockman, W. T., & Jackson, R. B. (2004). Adaptive variation in the vulnerability of woody plants to xylem cavitation. *Ecology*, *85*(8), 2184–2199. https://doi.org/10.1890/02-0538

Martin-StPaul, N., Delzon, S., & Cochard, H. (2017). Plant resistance to drought depends on timely stomatal closure. *Ecology Letters*, *20*(11), 1437–1447.

Martínez-Vilalta, J., Poyatos, R., Aguadé, D., Retana, J., & Mencuccini, M. (2014). A new look at water transport regulation in plants. *New Phytologist*, *204*(1), 105–115.

Matsui, T., & Singh, B. (2003). Root characteristics in cowpea related to drought tolerance at the seedling stage. *Experimental Agriculture*, *39*(1), 29–38. https://doi.org/10.1017/s0014479703001108

McDowell, N. G., & Allen, C. D. (2015). Darcy's law predicts widespread forest mortality under climate warming. *Nature Climate Change*, *5*(7), 669–672. https://doi.org/10.1038/nclimate2641

Meinzer, F. C., Woodruff, D. R., Marias, D. E., McCulloh, K. A., & Sevanto, S. (2014). Dynamics of leaf water relations components in co-occurring iso-and anisohydric conifer species. *Plant, Cell and Environment*, *37*(11), 2577–2586. https://doi.org/10.1111/pce.12327

Mencuccini, M. (2003). The ecological significance of long-distance water transport: Short-term regulation, long-term acclimation and the hydraulic costs of stature across plant life forms. *Plant, Cell and Environment*, *26*(1), 163–182. https://doi.org/10.1046/j.1365-3040.2003.00991.x

Milly, P. C., & Dunne, K. A. (2016). Potential evapotranspiration and continental drying. *Nature Climate Change*, *6*(10), 946–949. https://doi.org/10.1038/nclimate3046

Miralles, D., Jiménez, C., Jung, M., Michel, D., Ershadi, A., McCabe, M., et al. (2016). The WACMOS-ET project-Part 2: Evaluation of global terrestrial evaporation data sets. *Hydrology and Earth System Sciences*, *20*(2), 823–842. https://doi.org/10.5194/hess-20-823-2016

Miralles, D. G., Gentine, P., Seneviratne, S. I., & Teuling, A. J. (2018). Land–atmospheric feedbacks during droughts and heatwaves: State of the science and current challenges. *Annals of the New York Academy of Sciences*, *1436*(1), 19–35.

Momen, M., Wood, J. D., Novick, K. A., Pangle, R., Pockman, W. T., McDowell, N. G., & Konings, A. G. (2017). Interacting effects of leaf water potential and biomass on vegetation optical depth. *Journal of Geophysical Research: Biogeosciences*, *122*(11), 3031–3046. https://doi.org/10.1002/2017jg004145

Mooney, H., Field, C., Yanes, C. V., & Chu, C. (1983). Environmental controls on stomatal conductance in a shrub of the humid tropics. *Proceedings of the National Academy of Sciences*, *80*(5), 1295–1297. https://doi.org/10.1073/pnas.80.5.1295

Nardini, A., Casolo, V., Borgo, Dal, A., Savi, T., Stenni, B., Bertoncin, P., et al. (2016). Rooting depth, water relations and non-structural carbohydrate dynamics in three woody angiosperms differentially affected by an extreme summer drought. *Plant, Cell & Environment*, *39*(3), 618–627. https://doi.org/10.1111/pce.12646

Nepstad, D. C., Carvalho, de, C. R., Davidson, E. A., Jipp, P. H., Lefebvre, P. A., Negreiros, G. H., et al. (1994). The role of deep roots in the hydrological and carbon cycles of Amazonian forests and pastures. *Nature*, *372*(6507), 666–669. https://doi.org/10.1038/372666a0

Novick, K. A., Konings, A. G., & Gentine, P. (2019). Beyond soil water potential: An expanded view on isohydricity including land–atmosphere interactions and phenology. *Plant, Cell & Environment*, *42*(6), 1802–1815. https://doi.org/10.1111/pce.13517

Pan, Y., Birdsey, R. A., Fang, J., Houghton, R., Kauppi, P. E., Kurz, W. A., et al. (2011). A large and persistent carbon sink in the world's forests. *Science*, *333*, 988–993. https://doi.org/10.1126/science.1201609

Pangle, R. E., Limousin, J. M., Plaut, J. A., Yepez, E. A., Hudson, P. J., Boutz, A. L., et al. (2015). Prolonged experimental drought reduces plant hydraulic conductance and transpiration and increases mortality in a piñon–juniper woodland. *Ecology and Evolution*, *5*(8), 1618–1638. https://doi.org/10.1002/ece3.1422

Pastorello, G., Trotta, C., Canfora, E., Chu, H., Christianson, D., Cheah, Y. W., et al. (2020). The FLUXNET2015 dataset and the ONEFlux processing pipeline for eddy covariance data. *Scientific Data*, *7*, 1–27.

Phillips, N., Ryan, M., Bond, B., McDowell, N., Hinckley, T., & Čermák, J. (2003). Reliance on stored water increases with tree size in three species in the Pacific Northwest. *Tree Physiology*, *23*(4), 237–245. https://doi.org/10.1093/treephys/23.4.237

Pinheiro, H. A., DaMATTA, F. M., Chaves, A. R., Loureiro, M. E., & Ducatti, C. (2005). Drought tolerance is associated with rooting depth and stomatal control of water use in clones of Coffea canephora. *Annals of Botany*, *96*(1), 101–108. https://doi.org/10.1093/aob/mci154

Reich, P. B., & Borchert, R. (1988). Changes with leaf age in stomatal function and water status of several tropical tree species. *Biotropica*, *20*, 60–69. https://doi.org/10.2307/2388427

Rodell, M., Houser, P., Jambor, U., Gottschalck, J., Mitchell, K., Meng, C.-J., et al. (2004). The global land data assimilation system. *Bulletin of the American Meteorological Society*, *85*(3), 381–394. https://doi.org/10.1175/bams-85-3-381

Sack, L., & Holbrook, N. M. (2006). Leaf hydraulics. *Annual Review of Plant Biology*, *57*, 361–381. https://doi.org/10.1146/annurev.arplant.56.032604.144141

Salehi-Lisar, S. Y., & Bakhshayeshan-Agdam, H. (2016). Drought stress in plants: Causes, consequences, and tolerance. In *Drought Stress Tolerance in Plants Physiology and Biochemistry* (Vol. 1, pp. 1–16). Springer. https://doi.org/10.1007/978-3-319-28899-4_1

Samanta, A., Knyazikhin, Y., Xu, L., Dickinson, R. E., Fu, R., Costa, M. H., et al. (2012). Seasonal changes in leaf area of Amazon forests from leaf flushing and abscission. *Journal of Geophysical Research: Biogeosciences*, *117*(G1), G01015. https://doi.org/10.1029/2011jg001818

Santos, V. A. H. F. D., Ferreira, M. J., Rodrigues, J. V. F. C., Garcia, M. N., Ceron, J. V. B., Nelson, B. W., & Saleska, S. R. (2018). Causes of reduced leaf-level photosynthesis during strong El Niño drought in a Central Amazon forest. *Global Change Biology*, *24*(9), 4266–4279

Saxton, K., Rawls, W. J., Romberger, J., & Papendick, R. (1986). Estimating generalized soil-water characteristics from texture 1. *Soil Science Society of America Journal*, *50*(4), 1031–1036. https://doi.org/10.2136/sssaj1986.03615995005000040039x

Schenk, H., & Jackson, R. (2003).*Global distribution of root profiles in terrestrial ecosystems*. ORNL DAAC.

Schenk, H. J., & Jackson, R. B. (2002). The global biogeography of roots. *Ecological Monographs*, *72*(3), 311–328. https://doi.org/10.1890/0012-9615(2002)072[0311:tgbor]2.0.co;2

Schenk, H. J., Jackson, R. B., Hall, F. G., Collatz, G. J., Meeson, B. W., Los, S. O., et al. (2009). *ISLSCP II ecosystem rooting depths*. ORNL DAAC. https://doi.org/10.3334/0RNLDAAC/929

Sellin, A. (1999). Does pre-dawn water potential reflect conditions of equilibrium in plant and soil water status? *Acta Oecologica*, *20*(1), 51–59. https://doi.org/10.1016/s1146-609x(99)80015-0

Simard, M., Pinto, N., Fisher, J. B., & Baccini, A. (2011). Mapping forest canopy height globally with spaceborne lidar. *Journal of Geophysical Research: Biogeosciences*, *116*(G4), G04021. https://doi.org/10.1029/2011jg001708

Sinclair, T. R., & Muchow, R. C. (2001). System analysis of plant traits to increase grain yield on limited water supplies. *Agronomy Journal*, *93*(2), 263–270. https://doi.org/10.2134/agronj2001.932263x

Sofo, A., Manfreda, S., Fiorentino, M., Dichio, B., & Xiloyannis, C. (2008). The olive tree: A paradigm for drought tolerance in Mediterranean climates. *Hydrology and Earth System Sciences Discussions*, *12*(1), 293–301. https://doi.org/10.5194/hess-12-293-2008

Sperry, J. S., & Love, D. M. (2015). What plant hydraulics can tell us about responses to climate-change droughts. *New Phytologist*, *207*(1), 14–27. https://doi.org/10.1111/nph.13354

Subramanian, K., Santhanakrishnan, P., & Balasubramanian, P. (2006). Responses of field grown tomato plants to arbuscular mycorrhizal fungal colonization under varying intensities of drought stress. *Scientia Horticulturae*, *107*(3), 245–253. https://doi.org/10.1016/j.scienta.2005.07.006

Taiz, L., & Zeiger, E. (2010). *Plant physiology* (5th ed.). Sinauer Associates.

Teuling, A., Seneviratne, S. I., Williams, C., & Troch, P. (2006). Observed timescales of evapotranspiration response to soil moisture. *Geophysical Research Letters*, *33*(23), L23403. https://doi.org/10.1029/2006gl028178

Trugman, A., Medvigy, D., Mankin, J., & Anderegg, W. (2018). Soil moisture stress as a major driver of carbon cycle uncertainty. *Geophysical Research Letters*, *45*, 6495–6503. https://doi.org/10.1029/2018GL078131

Van Emmerik, T., Steele-Dunne, S. C., Judge, J., & Van De Giesen, N. (2016). Dielectric response of corn leaves to water stress. *IEEE Geoscience and Remote Sensing Letters*, *14*(1), 8–12.

Viterbo, P., & Beljaars, A. C. (1995). An improved land surface parameterization scheme in the ECMWF model and its validation. *Journal of Climate*, *8*(11), 2716–2748. https://doi.org/10.1175/1520-0442(1995)008<2716:ailsps>2.0.co;2

Wu, J., Albert, L. P., Lopes, A. P., Restrepo-Coupe, N., Hayek, M., Wiedemann, K. T., et al. (2016). Leaf development and demography explain photosynthetic seasonality in Amazon evergreen forests. *Science*, *351*(6276), 972–976. https://doi.org/10.1126/science.aad5068

Xu, X., Medvigy, D., Powers, J. S., Becknell, J. M., & Guan, K. (2016). Diversity in plant hydraulic traits explains seasonal and inter-annual variations of vegetation dynamics in seasonally dry tropical forests. *New Phytologist*, *212*(1), 80–95. https://doi.org/10.1111/nph.14009

Yang, Y., Donohue, R. J., & McVicar, T. R. (2016). Global estimation of effective plant rooting depth: Implications for hydrological modeling. *Water Resources Research*, *52*(10), 8260–8276. https://doi.org/10.1002/2016wr019392

Zhang, Y., Zhou, S., Gentine, P., & Xiao, X. (2019). Can vegetation optical depth reflect changes in leaf water potential during soil moisture dry-down events? *Remote Sensing of Environment*, *234*, 111451. https://doi.org/10.1016/j.rse.2019.111451

Zhao, M., & Running, S. W. (2010). Drought-induced reduction in global terrestrial net primary production from 2000 through 2009. *Science*, *329*(5994), 940–943. https://doi.org/10.1126/science.1192666

Zhou, S., Williams, A. P., Berg, A. M., Cook, B. I., Zhang, Y., Hagemann, S., et al. (2019). Land–atmosphere feedbacks exacerbate concurrent soil drought and atmospheric aridity. *Proceedings of the National Academy of Sciences*, *116*(38), 18848–18853. https://doi.org/10.1073/pnas.1904955116

References From the Supporting Information

Andela, N., Liu, Y., Dijk, Van, A., Jeu, De, R., & McVicar, T. (2013). Global changes in dryland vegetation dynamics (1988–2008) assessed by satellite remote sensing: Comparing a new passive microwave vegetation density record with reflective greenness data. *Biogeosciences*, *10*(10), 6657–6676. https://doi.org/10.5194/bg-10-6657-2013

McPherson, R. A., Fiebrich, C. A., Crawford, K. C., Kilby, J. R., Grimsley, D. L., Martinez, J. E., et al. (2007). Statewide monitoring of the mesoscale environment: A technical update on the Oklahoma Mesonet. *Journal of Atmospheric and Oceanic Technology*, *24*(3), 301–321. https://doi.org/10.1175/jtech1976.1

Rawls, W. J. (2004). Pedotransfer functions for the United States. *Developments in Soil Science*, *30*, 437–447. https://doi.org/10.1016/s0166-2481(04)30023-1